

Arabidopsis PPR40 Connects Abiotic Stress Responses to Mitochondrial Electron Transport^{1[W][OA]}

Laura Zsigmond, Gábor Rigó, András Szarka, Gyöngyi Székely, Krisztina Ötvös, Zsuzsanna Darula, Katalin F. Medzihradzky, Csaba Koncz, Zsuzsa Koncz, and László Szabados*

Institute of Plant Biology (L.Z., G.R., G.S., K.Ö., C.K., L.S.), and Proteomics Research Group (Z.D., K.F.M.), Biological Research Centre, Hungarian Academy of Sciences, 6726–Szeged, Hungary; Department of Applied Biotechnology and Food Science, Laboratory of Biochemistry and Molecular Biology, Budapest University of Technology and Economics, 1111–Budapest, Hungary (A.S.); Pathobiochemistry Research Group, Hungarian Academy of Sciences and Semmelweis University, 1111–Budapest, Hungary (A.S.); Department of Pharmaceutical Chemistry, University of California, San Francisco, California 94143–0446 (K.F.M.); and Max-Planck-Institut für Züchtungsforschung, D–50829 Cologne, Germany (C.K., Z.K.)

Oxidative respiration produces adenosine triphosphate through the mitochondrial electron transport system controlling the energy supply of plant cells. Here we describe a mitochondrial pentatricopeptide repeat (PPR) domain protein, PPR40, which provides a signaling link between mitochondrial electron transport and regulation of stress and hormonal responses in *Arabidopsis* (*Arabidopsis thaliana*). Insertion mutations inactivating PPR40 result in semidwarf growth habit and enhanced sensitivity to salt, abscisic acid, and oxidative stress. Genetic complementation by overexpression of *PPR40* complementary DNA restores the *ppr40* mutant phenotype to wild type. The PPR40 protein is localized in the mitochondria and found in association with Complex III of the electron transport system. In the *ppr40-1* mutant the electron transport through Complex III is strongly reduced, whereas Complex IV is functional, indicating that PPR40 is important for the ubiquinol-cytochrome *c* oxidoreductase activity of Complex III. Enhanced stress sensitivity of the *ppr40-1* mutant is accompanied by accumulation of reactive oxygen species, enhanced lipid peroxidation, higher superoxide dismutase activity, and altered activation of several stress-responsive genes including the alternative oxidase *AOX1d*. These results suggest a close link between regulation of oxidative respiration and environmental adaptation in *Arabidopsis*.

Adaptation of plants to environmental stresses has important metabolic implications, including changes in photosynthesis, respiration, metabolite assimilation, and catabolism. Mitochondria are in the center of regulation of cellular energy homeostasis and redox balance, and integrate numerous metabolic pathways that are important in adaptive responses to extreme environmental conditions. Respiration and oxidative phosphorylation; metabolism of Pro, Cys, ascorbate, and folate; and the control of redox balance are exam-

ples of processes illustrating the importance of mitochondria in coordination of cellular metabolism during stress adaptation (Sweetlove et al., 2007).

Respiration is the core process of mitochondrial metabolism in which a large amount of free energy is released and used for ATP production. During respiration, controlled oxidation of reduced carbohydrates, such as malate and pyruvate, takes place through glycolysis and tricarboxylic acid cycle producing, respectively, reducing NADPH and FADH₂. Electrons from the NADPH and FADH₂ are transferred to O₂ via the electron transport chain generating the energy carrier ATP and oxidized NADP⁺ and FAD⁺ (Siedow and Day, 2000). As in animal mitochondria, the plant electron transport system is composed of five respiratory complexes, which form supercomplexes (Dudkina et al., 2006). Depending on the substrate, electrons are transported from Complex I (NADH dehydrogenase) and Complex II (succinate dehydrogenase) through ubiquinone and Complex III (cytochrome *c* reductase) to cytochrome *c* and to Complex IV (cytochrome *c* oxidase [COX]), which produces water. In the energy conserving pathway, ATP is generated by Complex V (ATP synthase). However, plant respiratory metabolism can also utilize alternative glycolytic, phosphorylating, and electron transport pathways. When the electron transport in the cytochrome *c*

¹ This work was supported by the European Union FP5 (grant no. QLRT-2001-00841), NKFP (grant no. 4-038-04), OTKA (grant no. T-046552), and the joint research project (DFG 436UNG 13/172/01) between the Deutsche Forschungsgemeinschaft and the Hungarian Academy of Sciences. The Proteomics Research Group was supported by the Hungarian National Office for Research and Technology (RET-08/2004) and OTKA (grant no. K-60283). The Semmelweis University research group was supported by OTKA (grant no. 69187).

* Corresponding author; e-mail szabados@brc.hu.

The author responsible for distribution of materials integral to the findings presented in this article in accordance with the policy described in the Instructions for Authors (www.plantphysiol.org) is: László Szabados (szabados@brc.hu).

^[W] The online version of this article contains Web-only data.

^[OA] Open Access articles can be viewed online without a subscription.

www.plantphysiol.org/cgi/doi/10.1104/pp.107.111260

pathway is blocked, alternative oxidases (AOXs) help to maintain the electron flux and functional tricarboxylic acid cycle, even in the absence of oxidative phosphorylation (Vanlerberghe and Ordog, 2002; Plaxton and Podestá, 2006). Thus, under stress the mitochondrial electron transport relies on the functions of AOXs, which can bypass the blocked proton pumping Complex III (Vanlerberghe and Ordog, 2002). Besides maintenance of electron flux, AOXs can reduce the reactive oxygen species (ROS) levels in situations when Complexes III and IV are unable to function properly. Such flexibility in plant respiration is considered to be an essential mechanism at the biochemical level, which provides plants with the capability to adapt better to stress conditions, such as low temperature, salinity, drought, oxidative stress, heavy metal exposure, hypoxia, nutrient deprivation, wounding, and pathogen infection (Møller, 2001; Plaxton and Podestá, 2006).

Mitochondrial electron transport is also important to neutralize the excess of reducing capacity of photosynthesis, preventing oxidative damage of thylakoid membranes and other cellular components (Møller, 2001; Raghavendra and Padmasree, 2003). ROS are produced in the mitochondrial electron transport chain, where Complex I (NADH dehydrogenase) and Complex III (ubiquinol-cytochrome bc_1 reductase) are major sites for ROS synthesis in the darkness and in nongreen tissues. Mitochondrial electron transport is implicated in ROS production during different biotic and abiotic stresses (Møller, 2001; Navrot et al., 2007). ROS can oxidize and damage cellular structures, macromolecules, nucleic acids, proteins, and lipids. Besides being damaging agents, ROS are important signaling compounds implicated in the control of plant development, adaptation to environmental stress conditions, defense, and programmed cell death. In interaction with other signaling molecules (e.g. lipid signals, nitrogen oxide, calcium ions, and plant hormones) ROS control protein stability and gene expression (Desikan et al., 2001; Laloi et al., 2004; Gechev et al., 2006). During drought, for example, stomatal closure and other stress responses are regulated by abscisic acid (ABA) through interaction with H_2O_2 signals (Leung and Giraudat, 1998; Finkelstein and Rock, 2002).

Mitochondrial proteins encoded in the nucleus are imported by a specialized organelle transport system. A particular nuclear encoded organellar protein family is characterized by 9 to 15 tandem arrays of pentatricopeptide repeats (PPRs), which are composed of degenerate 35 amino acid units (Small and Peeters, 2000). PPRs form helical structures and are considered to be RNA-binding motifs (Lurin et al., 2004). PPR domains are related to tetratricopeptide repeats, which mediate protein-protein interactions, suggesting that PPR domains may also perform similar functions (Blatch and Lässle, 1999; Small and Peeters, 2000). The PPR domain protein family is particularly large in plants. In the *Arabidopsis thaliana* genome, 441 putative PPR genes were identified (Lurin

et al., 2004), but only six of them have been characterized in detail (Andrés et al., 2007). Altogether, the biological function of no more than 20 plant PPR proteins is known (Andrés et al., 2007).

Posttranscriptional regulation of gene expression is a dominant mode of controlling gene activity in mitochondria. PPR proteins are implicated in the regulation of organellar gene expression by controlling diverse aspects of RNA metabolism, such as RNA splicing, editing, processing, and translation (Meierhoff et al., 2003; Williams and Barkan, 2003; Andrés et al., 2007). The PPR genes influence numerous biological processes including cytoplasmic male sterility (Desloire et al., 2003), circadian clock (Oguchi et al., 2004), seed development (Gutierrez-Marcos et al., 2007), and transcription and translation of plastid-encoded mRNAs and proteins, respectively (Meierhoff et al., 2003; Williams and Barkan, 2003). Embryo lethality, reduced fertility, and dwarf phenotype were associated as phenotypic traits with several PPR gene mutations highlighting important functions in the regulation of plant growth and development (Lurin et al., 2004; Gutierrez-Marcos et al., 2007). Here we describe novel functions of a PPR gene, which is implicated in mitochondrial electron transport and thereby influences growth, abiotic stress responses, and ABA sensitivity in *Arabidopsis*.

RESULTS

Isolation of *ppr40* Mutants

Screening of our T-DNA-tagged *Arabidopsis* collection (Szabados et al., 2002) for mutations causing altered hormonal responses yielded an ABA hypersensitive mutant that showed semidwarf growth habit (Fig. 1, A and B). Characterization of this insertional mutation identified a tandem inverted (LB-RB/RB-LB) T-DNA repeat in the transcribed region of gene *At3g16890*. The T-DNA insertion caused a target site deletion of 4 bp and was localized 311 bp downstream of the predicted ATG codon (Fig. 1A). In the Salk Institute mutant collection (<http://signal.salk.edu/cgi-bin/tdnaexpress>), we identified a second mutant allele (SALK_071712), in which the T-DNA insertion occurred 852 bp downstream of the ATG causing a deletion of 5 bp (Fig. 1A).

The *At3g16890* gene has a single exon with an open reading frame (ORF) of 1,980 bp and encodes a 74-kD protein composed of 659 amino acid residues (Fig. 1D). The *At3g16890* protein belongs to the P subclass of the PPR protein family and was previously named PPR40 (PPR model, PPR_3_5768407; Lurin et al., 2004). The PPR40 protein carries a predicted mitochondrial targeting signal and 14 conserved PPR motifs arranged in two separate domains (Fig. 1, D and F). In different plant species, genome sequencing revealed a large number of PPR domain proteins (Lurin et al., 2004). PPR40 orthologs sharing highly conserved domain structure have been identified in *Vitis* and rice (*Oryza sativa*; Supplemental Fig. S1).

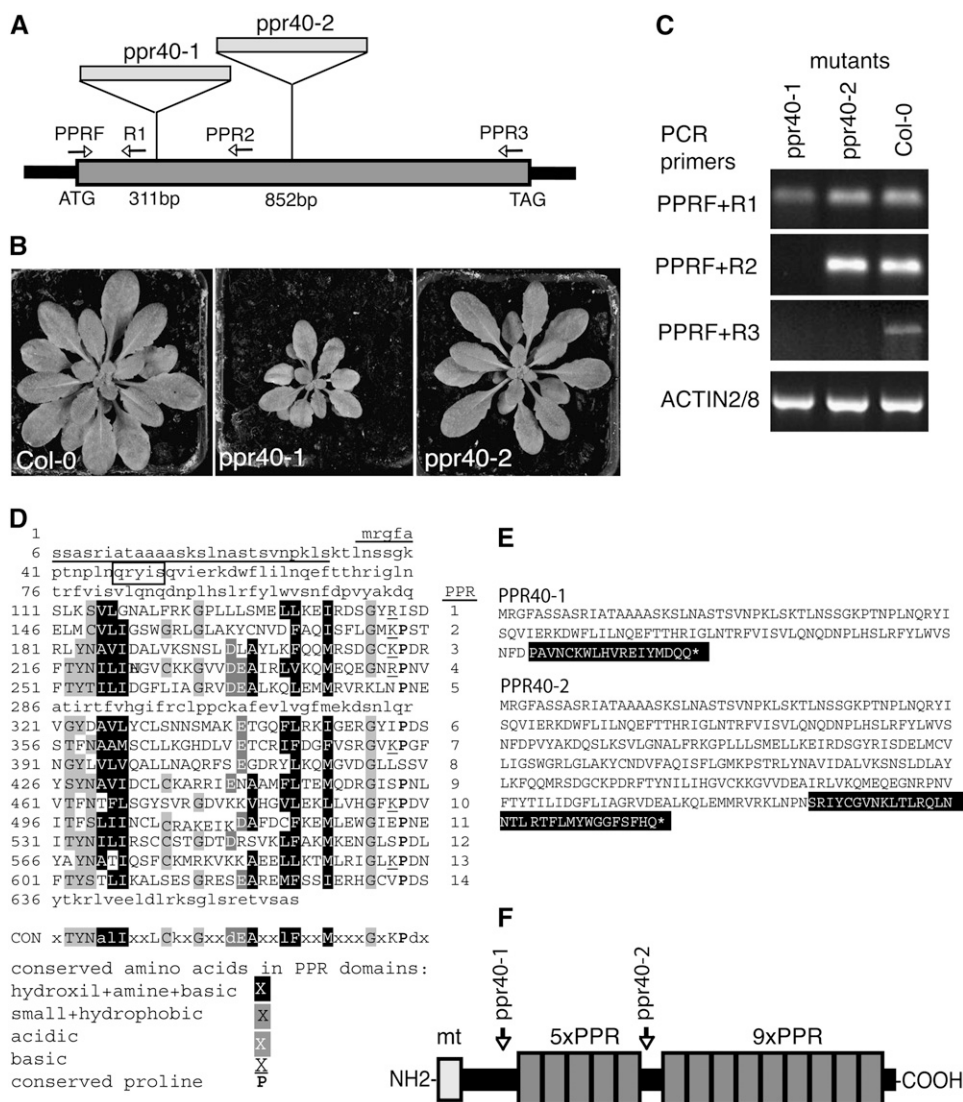


Figure 1. Characterization of *ppr40-1* and *ppr40-2* T-DNA insertion mutations and predicted structure of truncated PPR40 proteins in the mutants. **A**, Positions of T-DNA insertions in the *At3g16890* gene. The coding sequence is disrupted by an inverted T-DNA repeat located downstream of the ATG codon at positions 311 bp in the *ppr40-1* allele and by a T-DNA at position 852 bp in the *ppr40-2* allele (SALK_071712). The positions of gene-specific PCR primers (PPRF and PPR-R1, PPR-R2, and PPR-R3) used for RT-PCR and testing the segregation of T-DNA insertions by RT-PCR are shown by arrows. **B**, Rossette phenotype of 4-week-old wild type, and *ppr40-1* and *ppr40-2* mutant plants grown in greenhouse conditions. **C**, RT-PCR analysis PPR40 transcripts in *ppr40-1*, *ppr40-2*, and wild-type (Col-0) plants. Various primer combinations were used to amplify different fragments of *At3g16890* cDNA to distinguish transcribed PPR40 sequences in wild type and *ppr40* mutants, and ACTIN2/8 primers were used as a reference for template concentration. **D**, Predicted amino acid sequence of the PPR40 protein. Putative mitochondrial targeting signal is underlined, the predicted cleavage site (qryis) is framed. PPR domains are aligned and numbered from 1 to 14. Conserved amino acid motifs in the PPR domains are highlighted and their consensus sequence is shown below (CON). **E**, Predicted amino acid sequences of truncated PPR40 proteins that are possibly produced in the *ppr40-1* and *ppr40-2* mutants. Highlighted regions indicate sequences encoded by the T-DNA inserts yielding C-terminal fusions with the predicted PPR40-1 and PPR40-2 proteins. **F**, Domain structure of the PPR40 protein. Mitochondrial targeting signal (mt) and the two PPR repeat domains (5 × PPR, 9 × PPR) are indicated. Arrows mark the end of PPR40 sequences in the predicted PPR40-1 and PPR40-2 proteins.

Reverse transcription (RT)-PCR analysis indicated the lack of full-length *At3g16890* transcript in the homozygous *ppr40-1* and *ppr40-2* mutants (Fig. 1C). However, 3'-truncated transcripts from both mutant alleles were detected with primers PPRF+PPRR1 positioned 5' upstream of the *ppr40-1* T-DNA insertion

site. Primers PPRF+PPRR2 positioned upstream of the *ppr40-2* insertion detected truncated transcripts only in the *ppr40-2* mutant (Fig. 1C). The RT-PCR analysis thus suggested that C-terminally truncated proteins may be produced in both *ppr40-1* and *ppr40-2* mutants. The *ppr40-1* allele allows theoretically the synthesis of a

truncated protein of 121 amino acids composed of 103 residues encoded by the *PPR40* coding region and 18 C-terminal amino acids encoded by T-DNA sequences. If produced, this truncated PPR40-1 protein carries only the mitochondrial targeting signal without PPR sequences. On the other hand, the truncated PPR40-2 protein of 318 amino acids is predicted to contain 284 *PPR40*-encoded amino acids followed by 34 T-DNA encoded C-terminal amino acids (Fig. 1, D and E). Although so far no evidence supports the existence of these truncated proteins in the *ppr40* mutants, the fact that the *ppr40-2* mutant shows less severe growth retardation than *ppr40-1* (Fig. 1B; see below) suggests possible synthesis of the truncated ppr40-2 protein resulting in a partial loss of function phenotype.

Data deposited in microarray transcript profiling databases indicate that the *PPR40* gene is constitutively transcribed at low levels in all tissue types throughout plant development and not regulated by any thus far recorded treatment (<https://www.geneinvestigator.ethz.ch>). To verify these data, we examined the *PPR40* expression profile by quantitative RT-PCR (qRT-PCR) using RNA samples from different organs of wild-type plants. The *PPR40* transcript levels were almost three orders of magnitude lower than the reference *ACTIN2/8* mRNA in all tested tissues showing somewhat higher abundance in green siliques and seedlings (Supplemental Fig. S2). The level of *PPR40* transcript was not changed significantly by hormones (auxin, cytokinin, ethylene, and salicylic acid) and stress (salt, osmotic, and cold) treatments (data not shown).

ABA Hypersensitivity of *ppr40* Mutants

In comparison to wild type, the rosette size of the *ppr40-1* mutant was $50\% \pm 10\%$ ($n = 50$) smaller, whereas the *ppr40-2* mutant showed only a $20\% \pm 5\%$ ($n = 50$) reduction of rosette diameter during vegetative development (Fig. 1B). Both *ppr40* mutants were fertile and produced comparable amounts of seed as wild-type plants. The *ppr40* mutants displayed slightly delayed seed germination. Although germination of wild-type (ecotype Columbia of *Arabidopsis* [Col-0]) seed was 100% at day 4, the *ppr40-1* and *ppr40-2* mutants completed their germination with 2- and 1-d delays, respectively (Fig. 2B). Both *ppr40* mutants displayed enhanced, although different, degrees of sensitivity to inhibition of seed germination by ABA (Fig. 2A). In the presence of $0.5 \mu\text{M}$ ABA, only $20\% \pm 6\%$ of the *ppr40-1* seed germinated after 1 week compared to germination of $60\% \pm 3\%$ of the *ppr40-2* seed and $98\% \pm 2\%$ of the wild-type seed (in each case $n = 300$; Fig. 2B). Phenotypic differences in rosette growth and ABA sensitivity indicated that *ppr40-1* is likely a null allele, whereas *ppr40-2* represents a leaky mutation. Therefore, we used the *ppr40-1* allele in further characterization of *PPR40* function. Except ABA, other hormone responses of the *ppr40-1* mutant (e.g. auxin, cytokinin, ethylene, salicylic acid, GA, and brassinolide; Supplemental Table S1) were similar to the wild type.

Besides germination, ABA controls other physiological responses including stomatal opening, desiccation, plant growth, and expression of numerous genes. Stomatal closure is one of the most characteristic ABA-controlled responses during water deprivation. To compare ABA-induced stomatal closure of wild-type and *ppr40-1* plants, we prepared leaf epidermal peels from plants treated with different concentrations of ABA and recorded changes in the stomatal pore diameter. Whereas untreated wild-type and *ppr40-1* plants showed no significant difference, the *ppr40-1* mutant compared to the wild type responded with enhanced stomatal closure to increasing ABA concentrations (Fig. 2, C and D). Because stomatal closure affects the evaporation rate during drought, we have examined the water loss property of the *ppr40-1* mutant in desiccation assays. Water loss from isolated *ppr40-1* leaves was significantly lower compared to the wild type (Fig. 2E), correlating with enhanced ABA sensitivity of stomatal closure of the *ppr40-1* mutant.

To assess whether enhanced ABA sensitivity of *ppr40-1* correlates with either elevated ABA biosynthesis or alteration in signal transduction, we have first compared the free ABA concentrations in wild-type and *ppr40-1* seedlings exposed to treatment with 150 mM NaCl for 0, 6, and 24 h. The ABA levels were comparable in wild-type and *ppr40-1* seedlings cultured in medium without salt. Treatment for 6 h with 150 mM NaCl resulted in about a 50% increase of ABA content in both mutant and wild-type plants. Upon 24 h of salt treatment, however, the ABA concentration increased 3-fold in *ppr40-1* and 2.5-fold in wild type compared to untreated controls, suggesting that some increase in endogenous ABA levels during salt stress could contribute to the enhancement of stress sensitivity of the *ppr40-1* mutant (Fig. 2F).

To determine whether enhanced ABA and salt sensitivity of *ppr40-1* correlates with altered transcription of well-characterized stress-responsive genes acting in the parallel ABA-signaling pathways (Yamaguchi-Shinozaki and Shinozaki, 2005), we performed a series of qRT-PCR assays (Supplemental Fig. S3). The *ADH1* and *RAB18* transcript levels were similar in wild-type and *ppr40-1* plants. *RD22* showed higher, whereas *RD29A* had lower, transcript levels in the ABA-treated *ppr40-1* mutant compared to the wild type. On the other hand, mRNA levels of *DREB1B* and *DREB2B* transcription factors were comparable in untreated and ABA-treated wild-type and *ppr40-1* plants, but were significantly lower in the salt-treated *ppr40-1* mutant. Transcript levels of *MYB2* and *MYC2* (data not shown) transcription factor genes were similar in ABA-treated wild-type and *ppr40-1* plants, but were slightly lower in *ppr40-1* during salt stress. In *ppr40-1* seedlings, the mRNA level of *ABF1* transcription factor was higher after ABA and salt treatments. ABA induction of the SnRK1 α kinase *AKIN10* reached lower levels in *ppr40-1*, but mRNA levels of the seed-specific *ABI5* transcription factor did not reveal any significant difference. Despite detecting some increase in ABA

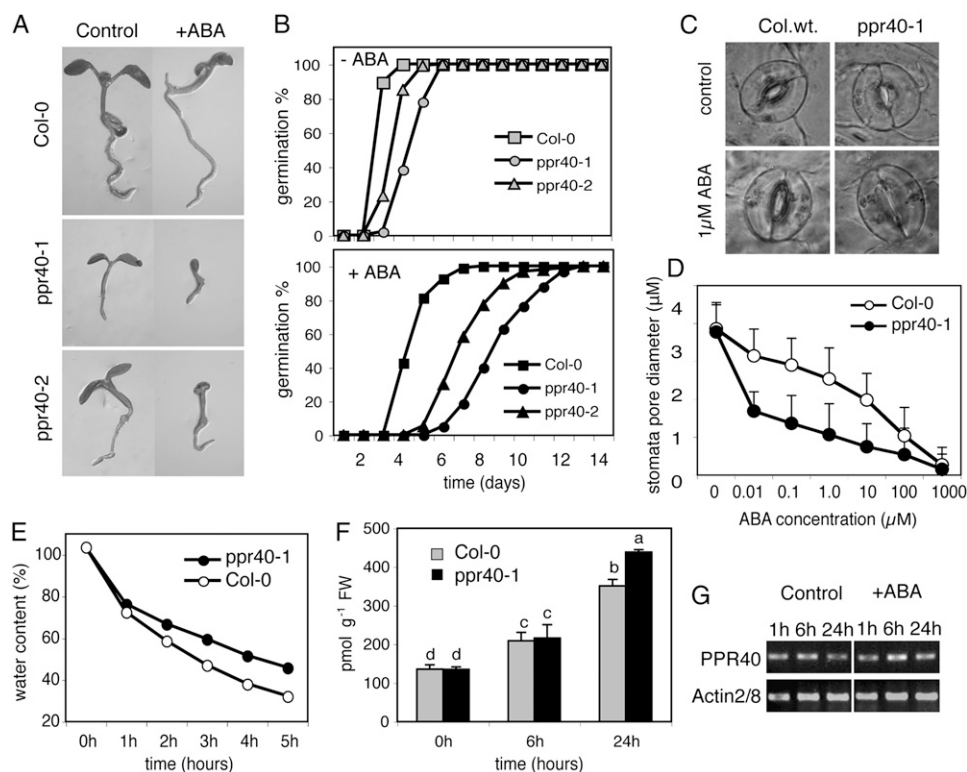


Figure 2. ABA responses of *ppr40* mutants. A, Analysis of ABA sensitivity of *ppr40-1* and *ppr40-2* mutants in germination assays. Wild-type (Col-0) and *ppr40* mutant seedlings following 6 d of germination in 0.5 Murashige and Skoog (MS) medium supplemented with 0.5 μM ABA. B, Germination kinetics of wild-type (Col-0), *ppr40-1*, and *ppr40-2* mutants seeds in the presence and absence of 0.5 μM ABA. C, Enhanced stomatal closure in *ppr40-1* epidermal layers indicates enhanced ABA sensitivity. Epidermal strips were floated on medium supplemented with different concentrations of ABA for 3 h. D, Pore size of stomata in ABA-treated wild-type (Col-0) and *ppr40-1* epidermal peels. Stomatal closure was quantified by measuring diameters of 80 stomata pores at each indicated ABA concentration. Calculated P value for the difference observed between the closure of wild-type and mutant stomata is $P < 0.0001$. E, Water loss of detached leaves of wild-type (Col-0) and *ppr40-1* mutant plants ($n = 50$; $P < 0.0001$). F, Internal ABA content of wild type and *ppr40-1* mutant seedlings. Three-week-old plantlets were treated with 200 mM NaCl for 0, 6, and 24 h, and internal the ABA content was determined by ELISA assay. Different letters indicate significant differences at $P < 0.05$ based on the Duncan test. G, Semiquantitative RT-PCR analysis of *PPR40* transcript levels in wild-type seedlings treated with either 0.5 MS medium or 0.5 MS containing 20 μM ABA for 1, 6, and 24 h. The *PPR40* cDNA was amplified using the primer combination PPRF+PPR3 (Fig. 1). ABA treatment led to no more than a 20% difference in *PPR40* transcript abundance.

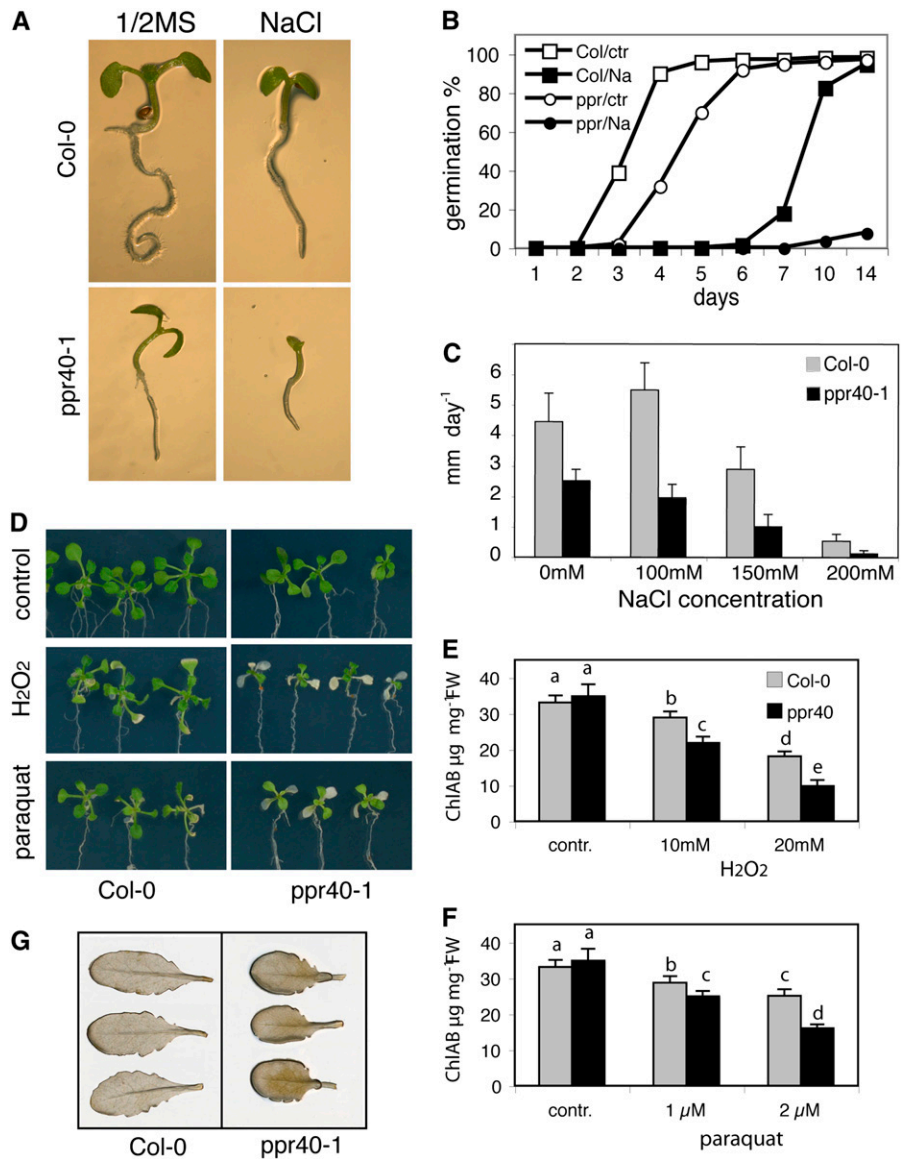
accumulation during salt stress and enhancement of ABA and salt sensitivity, these data indicated that the *PPR40* function was not implicated in the primary control of either ABA synthesis or signaling, although the *ppr40-1* mutation had some influence on these processes. Furthermore, transcription of *PPR40* was not altered by externally added ABA (Fig. 2G).

Environmental Stress Responses of *ppr40* Mutants

To test possible implication of *PPR40* in the regulation of plant responses to various environmental conditions and plant hormones, we performed seed germination and seedling growth assays (Supplemental Table S1). These indicated that in addition to ABA the *ppr40-1* mutant also shows enhanced sensitivity to salinity, osmotics, sugars, and oxidative stress. Germination of *ppr40-1* seeds was particularly inhibited by

NaCl (Fig. 3, A and B). Under standard conditions, the root growth rate of the *ppr40-1* mutant measured on vertical agar plates was 40% lower compared to wild type, whereas in the presence of 100 and 150 mM NaCl the *ppr40-1* root elongation rate of was, respectively, 65% to 75% lower than wild type. NaCl (200 mM) completely blocked root growth of the mutant, whereas wild-type roots continued to grow at a low rate at this salt concentration (Fig. 3C). Salt stress also caused lower fresh weight accumulation in the *ppr40-1* mutant compared to wild type (data not shown). The *ppr40-1* mutant showed enhanced sensitivity to oxidative stress. On media containing sublethal concentrations of either hydrogen peroxide or paraquat, the *ppr40-1* mutant displayed faster bleaching and chlorophyll degradation compared to the wild type (Fig. 3, D–F). This prompted us to test the accumulation of ROS, in particular hydrogen peroxide, in the *ppr40-1* mutant.

Figure 3. Salt and oxidative stress sensitivity of *ppr40-1* mutant. A, Seven-day-old *ppr40-1* and wild-type (Col-0) seedlings on media supplemented with 200 mM NaCl. B, Germination frequencies of *ppr40-1* (*ppr*) and wild-type (Col) seeds in the presence of 200 mM NaCl. ctr, One-half MS control medium; Na, 200 mM NaCl. C, Root growth of *ppr40-1* and wild-type (Col-0) plants on vertical agar plates supplemented with different concentrations of NaCl. Root growth rate of 50 plants was calculated from data collected every day throughout an observation period of 10 d. D to F, Enhanced oxidative damage in the *ppr40-1* mutant. Two-week-old wild-type (Col-0) and *ppr40-1* plants were treated with 10 mM H₂O₂ and 2 μM paraquat for 4 d (D). Compared to wild type (Col-0), leaves of the *ppr40-1* mutant show enhanced chlorosis. Diagrams (E and F) show reduction of chlorophyll levels in response to H₂O₂ and paraquat treatment throughout a period of 4 d, respectively. Different letters indicate significant differences at *P* < 0.05. G, Detection of hydrogen peroxide in leaves of wild-type (Col-0) and *ppr40-1* plants by DAB histochemical assay.



Histochemical 3,3-diaminobenzidine (DAB) assays indicated 28% ± 12% higher level of H₂O₂ accumulation in *ppr40-1* leaves (*P* < 0.0001; *n* = 50) suggesting that ROS damage could, at least partially, contribute to enhanced stress sensitivity of the mutant (Fig. 3G).

Genetic Complementation of the *ppr40-1* Mutation

The coding region of intronless *At3g16890* gene was PCR amplified and cloned into the pPILY intron-tagged hemagglutinine (HA)-epitope fusion vector (Ferrando et al., 2000). To perform genetic complementation, the *PPR40-HA* gene construct was inserted downstream of the cauliflower mosaic virus (CaMV) 35S promoter into the pBin19 vector (Bevan, 1984) and introduced into the *ppr40-1* mutant by *Agrobacterium*-mediated transformation. Six transgenic lines expressing PPR40-HA at high levels (Supplemental Fig. S2)

were subjected to further characterization. Semidwarf growth habit of the *ppr40-1* mutant was restored to the wild type in all examined genetically complemented *ppr40-1* lines similarly to *pprC/5* shown in Figure 4A. Salt sensitivity of the complemented plants was also similar to the wild type (Fig. 4, B and C). Furthermore, germination and growth of complemented *ppr40-1* lines were indistinguishable from the wild type on ABA-containing media (Fig. 4, D and E). These genetic complementation assays thus confirmed that the *ppr40-1* mutant phenotype was indeed caused by the T-DNA insertion mutation in the *At3g16890* gene.

Association of PPR40 with Mitochondrial Electron Transport

So far, all characterized PPR domain proteins have been localized in chloroplasts and mitochondria, and

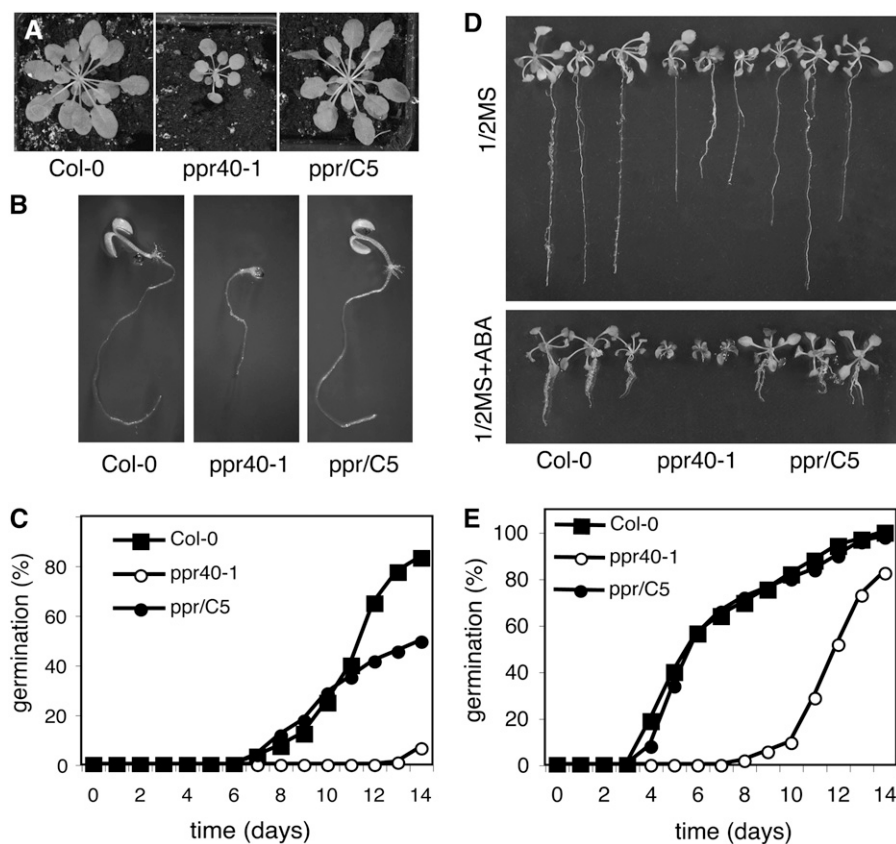


Figure 4. PPR40-HA expression by the CaMV 35S promoter complements the *ppr40-1* mutation. All complemented lines showed similar phenotype to *ppr40/C5*. A, Phenotype of 4-week-old wild type, *ppr40-1* mutant, and genetically complemented *ppr40/C5* line in soil. B, PPR40-HA expression restores the enhanced salt sensitivity trait of *ppr40-1* mutant to wild type. Ten-day-old wild type (Col-0), *ppr40-1* mutant, and genetically complemented *ppr/C5* seedlings germinated in the presence of 200 mM NaCl. C, Germination of wild type (Col-0), *ppr40-1* mutant, and complemented *ppr/C5* seeds on 0.5 MS medium containing 200 mM NaCl. D, Growth of the same lines on vertical plates for 2 weeks in the presence and absence of 1 μ M ABA. E, Germination efficiency of wild type (Col-0), *ppr40-1*, and *ppr/C5* seeds in the presence of 1 μ M ABA.

many of them are suggested to participate in the control of organellar gene expression (Andrés et al., 2007). Analysis of the PPR40 protein sequence by the TargetP program (<http://www.cbs.dtu.dk/services/TargetP>) suggested potential chloroplast localization, whereas the Predotar (<http://urgi.infobiogen.fr/predotar/>) and iPSORT algorithms (<http://psort.nibb.ac.jp/>) predicted mitochondrial targeting defining the position of a putative mitochondrial target peptide and cleavage site in the N-terminal region of PPR40 (Fig. 1D). To determine its intracellular localization, the presence of the PPR40-HA protein in different subcellular fractions was tested by western blotting using a monoclonal anti-HA antibody. Despite high levels of PPR40-HA mRNA, only low levels of the PPR40-HA protein were detected in total protein extracts prepared from the genetically complemented lines, but the protein was highly enriched in mitochondria compared to other cell organelles (Fig. 5A). Mitochondrial localization of the PPR40-HA protein was further analyzed by immunohistochemical detection of the HA epitope in cultured cells expressing the CaMV 35S-promoter-driven PPR40-HA construct. Confocal laser scanning microscopy indicated that the green fluorescence pattern of fluorescein isothiocyanate (FITC)-labeled anti-HA antibody (mouse monoclonal anti-HA antibody and FITC-conjugated goat anti-mouse IgG) and orange fluorescence pattern of the MitoTracker marker overlapped in the transformed

cells (Fig. 5B). High-resolution images revealed complete overlap of the two patterns confirming mitochondrial localization of PPR40 (Fig. 5C).

To search for possible function of PPR40, we have tested its RNA-binding capability using combined UV-formaldehyde cross-linking of mitochondrial protein-RNA complexes and RNA-binding gel shift assays with purified PPR40 and in vitro translated mitochondrial RNAs. However, these assays lead to negative results (data not shown). Therefore, we have investigated whether PPR40 is associated with protein complexes localized in mitochondrial membranes. Mitochondrial extracts purified from PPR40-HA-expressing cell cultures were subjected to fractionation of membrane proteins by Suc gradient centrifugation and blue-native PAGE (BN-PAGE). Suc gradient fractions were analyzed by BN-PAGE and western blotting using anti-HA antibody. Immunoblotting detected PPR40-HA in a protein complex of about 500 kD in the Suc gradient fractions 7 to 9 (Fig. 6A). The size of this complex corresponded to that of Complex III of mitochondrial electron transport system (Dudkina et al., 2005). To confirm association of PPR40-HA with Complex III, preparative two-dimensional BN-PAGE and SDS-PAGE was performed. Using this alternative separation method, PPR40-HA was also detected in Complex III by western blotting of preparative BN gels (Fig. 6B; western blotting of first dimension BN-PAGE). To analyze more precisely the composition of PPR40-

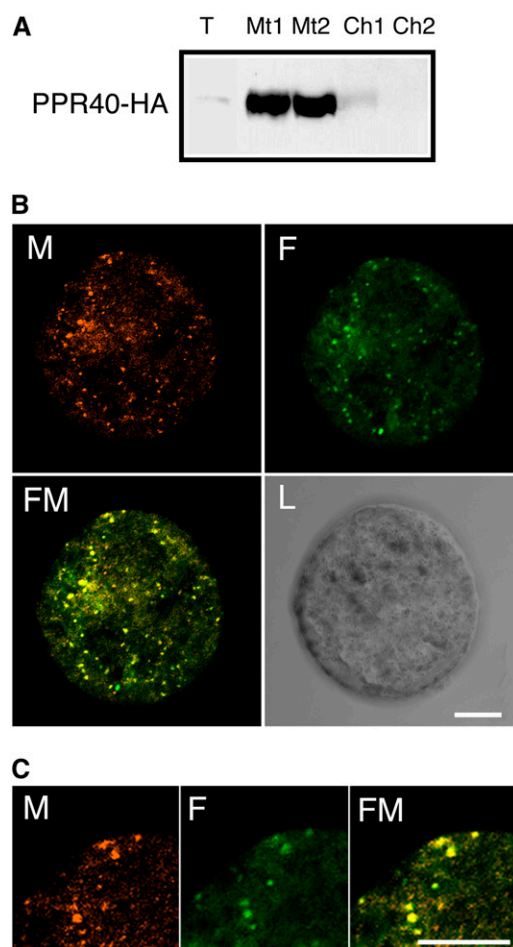


Figure 5. Cellular localization of PPR40-HA protein in mitochondria. A, Western-blot analysis of proteins from total cell extract (T), purified mitochondria (Mt), and chloroplast (Ch). HA-specific monoclonal antibody was used to detect the HA epitope-tagged PPR40-HA protein. The figure shows results of two independent cell fractionation experiments. B, Immunohistochemical localization of PPR40-HA protein in transformed *Arabidopsis* cells. Microphotographs show light image of a protoplast (L), green fluorescence of FITC-labeled anti-HA antibody (F), orange fluorescence of the MitoTracker orange marker (M), and merged fluorescence of FITC and MitoTracker (FM). C, High-resolution images of anti-HA FITC (F), MitoTracker (M), and overlay (FM) fluorescence signals. Bars, 5 μm .

HA-associated protein complex, the anti-HA cross-reacting protein complex was excised from the BN gel and size fractionated by SDS-PAGE. Subsequent western analysis confirmed that the excised complex indeed carried PPR40-HA of predicted molecular mass of 74 kD (Fig. 6B) in association with five major subunits of Complex III system that were identified by mass spectrometry (MS; Table I; Heazlewood et al., 2004).

To test whether the lack of PPR40 protein caused any alteration in the stoichiometry of core subunits of electron transport complexes, mitochondria were isolated from wild-type and *ppr40-1* mutant cell suspension cultures and membrane proteins were separated in BN gels. The respiratory complexes from wild-type

and mutant mitochondria showed similar BN gel resolution patterns (Fig. 7A; Supplemental Fig. S4A), and the stoichiometry of Complex III subunits analyzed by SDS-PAGE also appeared to be unaffected by the *ppr40-1* mutation (Fig. 7B; Supplemental Fig. S4B). Although PPR40 showed clear cofractionation with Complex III, these data indicated that PPR40 probably does not affect the composition and stability of core subunits of Complex III. Furthermore, the *ppr40-1* mutation did not appear to influence the transcript levels of genes coding for subunits of Complex III. qRT-PCR analysis of mRNA levels of these genes revealed no more than a 50% difference between the wild type and the *ppr40-1* mutant (Fig. 7C).

Apocytochrome B (*cob*, *ATMG00220*) is the only Complex III subunit that is encoded by the mitochondrial genome and is expressed as a 5-kb transcript (Brandt et al., 1993). All other Complex III subunits are encoded in nuclear genome and proteins are imported into mitochondria. To test whether PPR40 controls splicing of the apocytochrome B mRNA, northern hybridization of total mitochondrial RNA isolated from the wild type, the *ppr40-1* mutant, and the complemented mutant plants was performed. We observed no difference in *cob* transcript size between mutant, wild-type, and complemented plants (Fig. 7D). In addition, splicing of mitochondrially encoded intron-containing subunits of Complex I (*nad1*, *nad4*, and *nad7*) and Complex IV (*cox2* and *ccb452*) was tested by RT-PCR analysis and revealed no difference between wild-type, mutant, and complemented plants (data not shown). RNA editing of mitochondrial transcripts can influence gene activity. To test whether editing of apocytochrome B mRNA is different in the *ppr40-1* mutant, full-length *cob* complementary DNA (cDNA) was amplified and sequenced from RNA samples of wild-type, mutant, and complemented mutant plants. Sequence analysis could identify all seven *cob* C/U editing sites in each ORF as described by Giegé and Brennicke (1999), and confirmed that RNA editing did not change in the *ppr40-1* mutant (Supplemental Fig. S5).

Electron Transport of Complex III Is Compromised in the *ppr40-1* Mutant

Because the *ppr40-1* mutation did not appear to affect the subunit composition of respiratory complexes, we have asked the question whether PPR40 is required for proper control of respiration-associated mitochondrial functions, such as consumption of oxygen with different respiratory substrates and generation of ROS. Respiration was measured by oxygen consumption in mitochondria isolated from wild-type and *ppr40-1* mutant cell suspension cultures. Using NADH as the electron donor for Complex I, which is a major electron source in the respiration system, we observed 50% reduction of oxygen consumption in *ppr40-1* mitochondria compared to wild type (Fig. 8A). Similarly, application of succinate as electron donor for

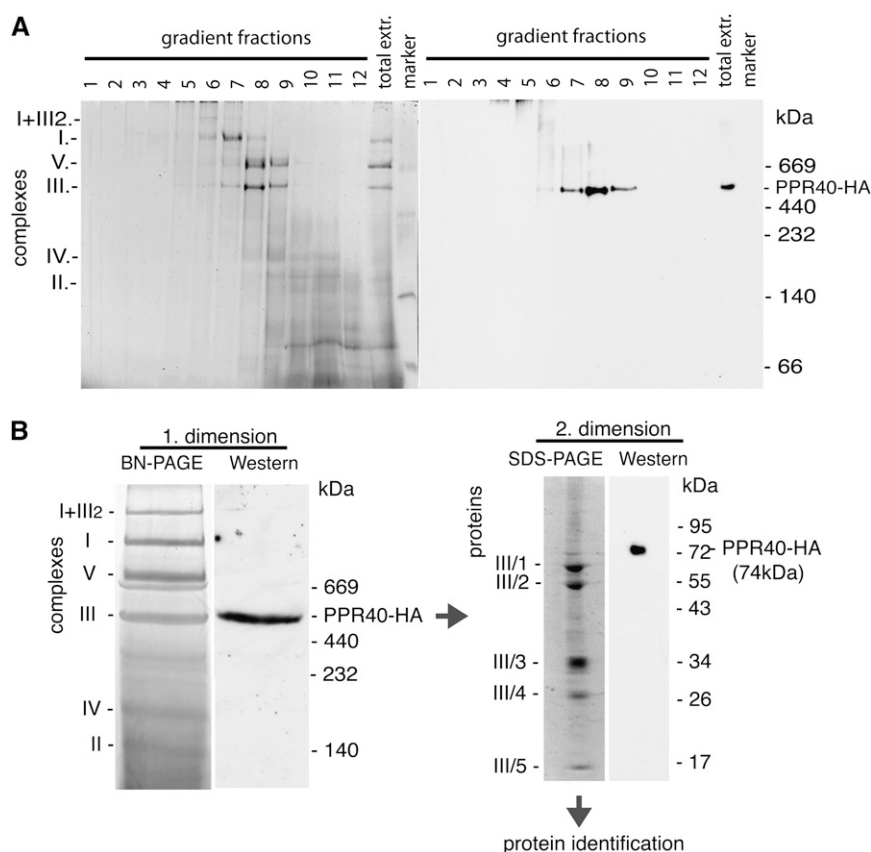


Figure 6. PPR40-HA is associated with Complex III of the mitochondrial electron transport system. **A**, Purified mitochondria were solubilized by digitonin, and protein complexes were separated by Suc gradient centrifugation. Aliquots of total protein extract (T) and Suc gradient fractions (1–12) were separated by BN-PAGE and subjected to western blotting with anti-HA IgG. PPR40-HA shows co-fractionation with the electron transport chain Complex III of 500 kD. **B**, Two-dimensional resolution of mitochondrial membrane complexes. Mitochondrial protein extract was separated in the first dimension by preparative BN-PAGE and subjected to western blotting with anti-HA IgG. Resolution of excised Complex III in the second dimension was performed by SDS-PAGE followed by western blotting to detect PPR40-HA. Coomassie staining of SDS-PAGE indicates substoichiometric association of PPR40-HA with Complex III. Identification of Complex III core subunits was performed by MS analysis (Table I). Molecular masses (kD) of standards are indicated.

Complex II that transfers electrons to Complex III via ubiquinone, revealed 40% lower oxygen consumption in *ppr40-1* mitochondria (Fig. 8A). These data indicated that electron transport through Complexes I and II, which act upstream of Complex III, was greatly reduced in the mutant.

During oxidative respiration Complex III transfers electrons from ubiquinol to cytochrome *c* (ubiquinol cytochrome *c* reductase activity) toward Complex IV, which has COX and mediates electron transfer to oxygen. Using ascorbate as respiratory substrate for Complex IV to measure direct electron transport from this substrate to oxygen, we detected 2.5- to 3.0-fold

higher oxygen consumption in *ppr40-1* mutant mitochondria compared to wild type (Fig. 8A). In contrast to reduced activities of Complexes I and II, this result indicated that Complex IV was fully functional and that ascorbate could at least partially bypass the defect of electron transport through Complex III in the *ppr40-1* mutant. Furthermore, we observed that COX activity was about twice as high in the *ppr40-1* mutant than in wild type (Fig. 8B), and the ascorbate consumption was 30% higher in roots and 80% higher in cell culture of the *ppr40-1* mutant compared to wild type (Fig. 8C). These data indicated that Complex IV worked at a higher rate in the *ppr40-1* mutant than in wild-type

Table I. List of proteins that were identified in the PPR40-HA-associated mitochondrial membrane complex

Each protein identified by MS corresponds to a subunit of Complex III of electron transport system.

Sample	Gene	Accession No.	Protein	Protein M_r	Unique Peptides	Coverage
1	At3g02090	Q42290	Mitochondrial-processing peptidase β -subunit (MPP β)	59	32	55.00%
1	At3g16480	O04308	Mitochondrial-processing peptidase α -subunit 2 (MPP α 2)	54	1 ^a	3.00%
1	At2g07727	P42792	Cytochrome <i>b</i> (MTCYB; COB; CYTB)	44.5	1 ^b	3.30%
2	At1g51980	Q9ZU25	Mitochondrial-processing peptidase α -subunit 1 (MPP α 1)	54 ^c	24	40.40%
2	At3g16480	O04308	Mitochondrial-processing peptidase α -subunit 2 (MPP α 2)	54 ^c	1 ^c (9)	16.40%
3	At5g40810	Q0WNJ4	Cytochrome <i>c</i> ₁ (CYC1-2)	33	6	20.80%
4	At5g13430	Q9LYR3	Ubiquinol-cytochrome <i>c</i> reductase (REISKE subunit)	26	6	22.10%
5	At4g32470	Q9SUU5	Ubiquinol-cytochrome <i>c</i> reductase complex 14-kD protein	14.5 ^d	5	49.20%
5	At5g25450	Q3E953	Ubiquinol-cytochrome <i>c</i> reductase complex 14-kD protein	14.6 ^d	1 ^d (2)	18.00%

^aEIEAIGGNTSASASR.

^bGIPNSYTDDETHT.

^cThese proteins feature 81% identity; however, there was a unique peptide (SAILmNLESR) detected for the α -subunit 2.

^dThese proteins feature about 81% identity; however, there was a unique peptide: SYLQDmLALVK detected for the second protein, too.

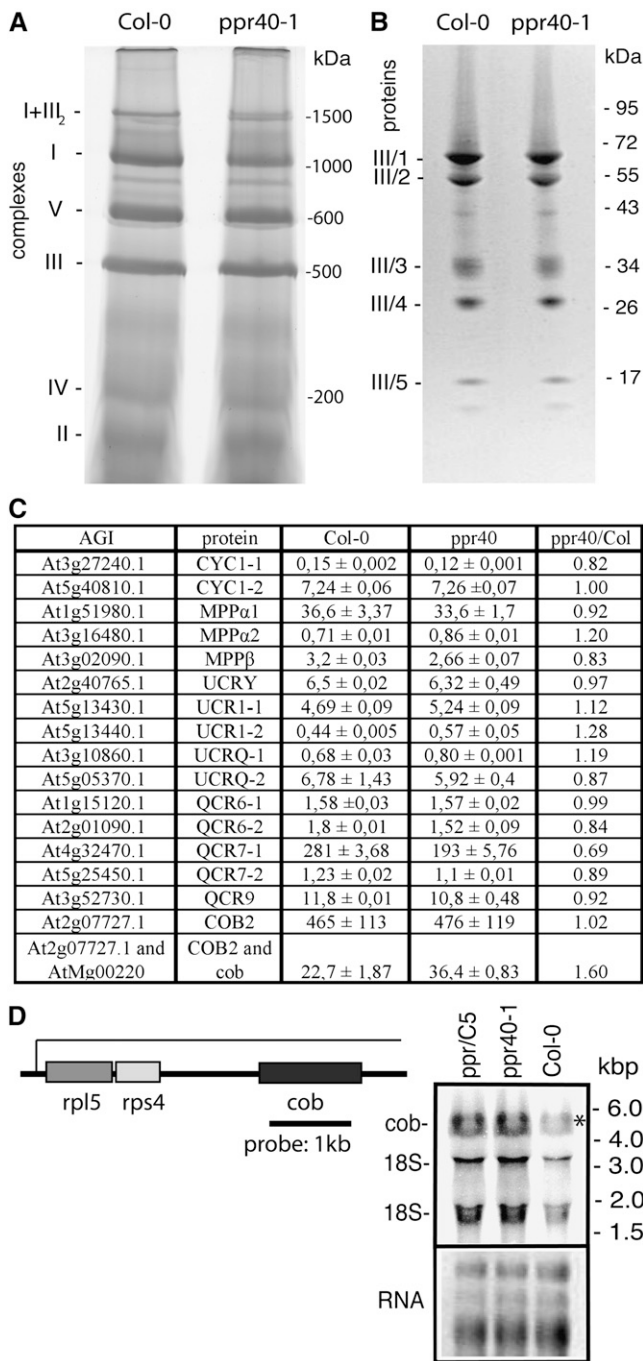


Figure 7. Mitochondrial respiratory complexes of wild type and the *ppr40-1* mutant show comparable BN and SDS-PAGE patterns. A, BN-PAGE resolution of membrane protein complexes of mitochondria isolated from wild-type and *ppr40-1* cell suspensions. B, SDS-PAGE analysis of Complex III excised from BN gels of wild-type and *ppr40-1* membrane complexes. C, qRT-PCR analysis of transcripts encoding Complex III subunits in wild-type (Col-0) and *ppr40-1* plants. The transcript levels were standardized to *GAPDH-2* control and the values were multiplied by 10³. CYC1-1 and CYC1-2, Cytochrome c₁ subunits 1 and 2; MPPα1, MPPα2, and MPPβ, mitochondrial processing peptidase α1, α2, and β-subunit; UCRY, ubiquinol cytochrome c reductase 6.7 kD subunit; UCR1-1 and UCR1-2, ubiquinol cytochrome c reductase REISKE subunit 1 and 2; UCRQ-1 and UCRQ-2, ubiquinol

mitochondria. Thus, despite remarkable reduction of electron transport through Complex III, the activity of Complex IV via ascorbate maintained a high level of oxygen consumption in the *ppr40-1* mutant.

Decreased ubiquinol cytochrome c reductase activity of Complex III results in hindered electron transport and accumulating electron pool, which can generate ROS. AOXs capture the excess electrons from ubiquinol, producing water and preventing accumulation of ROS during stress when electron transport through Complex III is reduced (Navrot et al., 2007). Our measurements showed that the AOX activity was 60% to 70% higher in the *ppr40-1* mutant compared to wild-type mitochondria (Fig. 8A). To determine whether AOX activation took place at the transcription level, the stress-responsive *AOX1d* transcript levels were compared in *ppr40-1* and wild-type plants. qRT-PCR analysis demonstrated that the *AOX1d* transcript levels were 15 to 20 times higher in the *ppr40-1* mutant than in wild-type and genetically complemented mutant plants (Fig. 8D). Salt treatment has enhanced *AOX1d* transcription, but also under these conditions the *AOX1d* transcript levels were 3 to 4 times higher in the *ppr40-1* mutant as in wild-type and genetically complemented plants. Enhanced induction of *AOX1D* transcription thus suggested the activation of the compensatory AOX pathway in *ppr40-1* mutant mitochondria.

Enhanced Oxidative Damage in the *ppr40-1* Mutant

Complexes I and III are considered to be main sources for generation of ROS in mitochondria during oxidative respiration (Chen et al., 2003; Navrot et al., 2007). Therefore, we have measured ROS accumulation and tested possible effects of oxidative damage in the *ppr40-1* mutant. Comparison of hydrogen peroxide production in mitochondria isolated from either roots or cultured cells of *ppr40-1* mutant, wild-type, and genetically complemented *ppr40-1* mutant indicated 30% higher H₂O₂ levels in *ppr40-1* mitochondria compared to controls, irrespective of source tissue examined (Fig. 9A).

Lipid peroxidation is a direct consequence of ROS damage and is therefore considered as major indication for ROS accumulation. In correlation with the higher level of hydrogen peroxide accumulation, we observed

cytochrome c reductase complex ubiquinone-binding protein 1 and 2; QCR6-1 and QCR6-2, ubiquinol-cytochrome c reductase 1 and 2; QCR7-1 and QCR7-2, ubiquinol cytochrome c reductase 14-kD subunits 1 and 2; QCR9, ubiquinol cytochrome c reductase 8-kD subunit; COB2, nuclear encoded apocytochrome B; cob, apocytochrome B; COB2 and cob, overlapping primers. D, Comparison of mRNA levels from the mitochondrial *rpl5-rps4-cob* operon using northern hybridization with an apocytochrome B (*cob*) probe of total mitochondrial RNA samples from the wild type (Col-0), the *ppr40-1* mutant, and complemented *ppr/C5* plants. The probe detects a 5-kb mRNA produced by the *rpl5-rps4-cob* operon at similar levels in all samples. Smaller hybridization signals result from artificial cross hybridization of 18S rRNA and its derivatives (Brandt et al., 1993). The bottom shows ethidium bromide stained RNA loading controls.

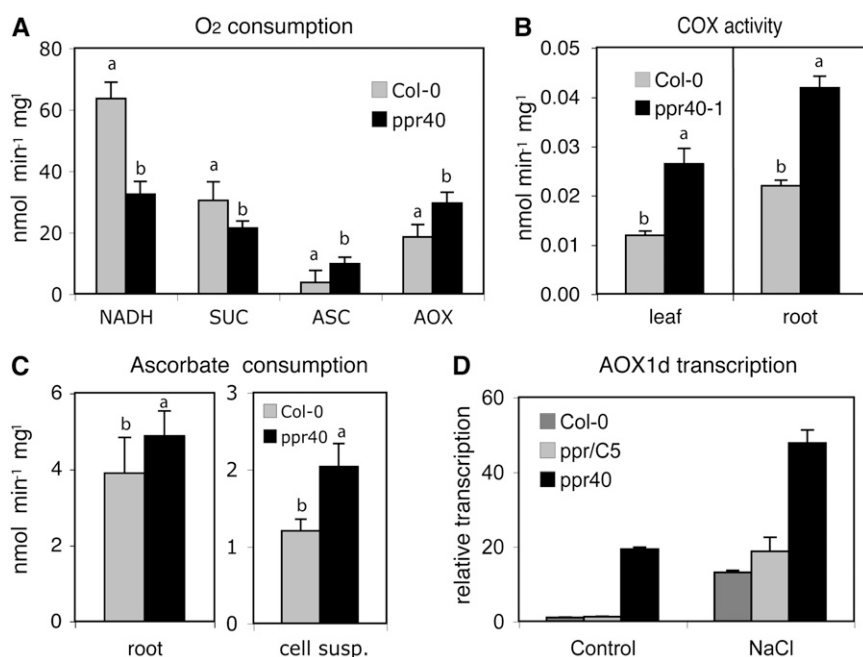


Figure 8. Electron transport through Complex III is compromised in the *ppr40-1* mutant. *A*, Oxygen consumption in mitochondria isolated from wild type (Col-0) and *ppr40-1* mutant cell cultures. NADH, succinate (suc), and ascorbate (asc) were used as electron donors, and oxygen consumption was monitored in isolated mitochondria. AOX capacity was measured in the presence of KCN to block the cytochrome *c* pathway. *B*, COX activity in leaves and roots of wild type (Col-0) and *ppr40-1* mutant plants ($P < 0.05$). *C*, Ascorbate consumption in wild type (Col-0) and *ppr40-1* mutant roots and cell suspensions. *D*, Relative transcript levels of the stress-responsive *AOX1d* gene in *ppr40-1*, genetically complemented *ppr/C5*, and wild-type (Col-0) plants subjected to treatment with 150 mM NaCl for 6 h. Control, plants without salt stress. The transcript levels are standardized relative to the *GAPDH-2* control.

that the ratio of oxidized lipids was 20% to 25% higher in leaves of the *ppr40-1* mutant compared to wild-type and genetically complemented mutant plants (Fig. 9B). Exposure to 150 mM NaCl salt stress for 24 h has slightly increased the level of lipid peroxidation, but the difference between *ppr40-1* and controls remained approximately the same as in nonstressed plants.

Superoxide radicals are known to be generated by Complex III misfunction during stress and represent the most damaging ROS species. Superoxide radicals are converted to H₂O₂ by mitochondrial manganese-containing superoxide dismutase (MnSOD; Navrot et al., 2007). We found that the SOD activity was 15% higher in leaves of the *ppr40-1* mutant compared to wild-type and genetically complemented mutant plants. However, this difference was more pronounced when MnSOD activity was measured in isolated mitochondria, which indicated 40% higher activity in *ppr40-1* than wild type (Fig. 9C). The observed increase of mitochondrial MnSOD activity therefore suggested enhanced generation of superoxide radicals and subsequent hydrogen peroxide accumulation in the *ppr40-1* mutant, which was in fact detected in our previous DAB assays. Therefore, enhanced sensitivity of the *ppr40-1* mutant to oxidative stress, which is accompanied by augmented salt and ABA sensitivity, likely reflects a result of elevated ROS generation by the damaged mitochondrial electron transport system.

DISCUSSION

Effects of the *ppr40-1* Mutation on Complex III in Mitochondrial Electron Transport

Our study documents that the function of PPR domain protein PPR40 is important for the ubiquinol-

cytochrome *c* reductase activity of Complex III in the mitochondrial electron transport chain, which has a significant influence on plant growth and responses to ABA and environmental stresses. This result adds a new aspect to the functional analysis of PPR domain proteins. PPRs located in chloroplasts and mitochondria are thought to interact with RNA and function in protein complexes as adaptors controlling either organellar RNA splicing and processing, or the stability of complex organelle structures (Williams and Barkan, 2003; Andrés et al., 2007). PPR and the related tetratricopeptide repeat domain proteins were reported to mediate protein-protein interactions in several pathways, including the regulation of ubiquitin conjugation and cell growth (Blatch and Lässle, 1999; Liu et al., 2005).

The *ppr40-1* mutation was originally identified in a genetic screen for mutants displaying enhanced sensitivity to ABA, but found later to confer delayed germination, semidwarf growth habit, and enhanced sensitivity to salt stress. Pleiotropic phenotype of the *ppr40-1* mutant thus indicates that inactivation of PPR40, which leads to altered mitochondrial electron transport, affects a wide range of cellular functions and stress responses. Other mutations influencing mitochondrial electron transport have been reported to cause growth defects (Newton and Coe, 1986; Gutierrez et al., 1997; Perales et al., 2005), cold hypersensitivity (Lee et al., 2002) and cytoplasmic male sterility (Newton and Coe, 1986). In particular, the *fro1* mutant impaired in the function of Complex I of the electron transport chain shows a remarkable reduction in cold-acclimation capacity and induction of stress-responsive genes (Lee et al., 2002). In general, many alterations in mitochondrial respiration are reported to affect cellular metabolism, plant growth, development,

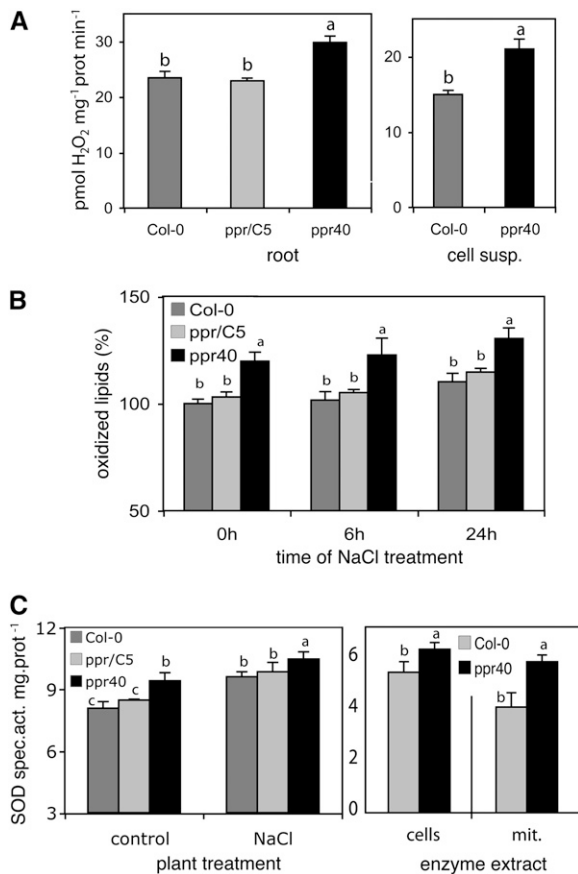


Figure 9. Accumulation of ROS in the *ppr40-1* mutant. A, H₂O₂ generation was measured in wild-type (Col-0), genetically complemented mutant (*ppr/C5*), and *ppr40-1* mutant mitochondria isolated from roots and cell suspensions. B, Measurement of lipid peroxidation in leaves of wild type (Col-0), *ppr40-1* mutant, and genetically complemented *ppr/C5* plants treated for 0, 6, and 24 h with 150 mM NaCl using the MDA assay (scale, nontreated wild-type level is 100%). C, SOD levels in protein extracts prepared from wild-type (Col-0), *ppr40-1* mutant, and genetically complemented *ppr/C5* plants, which were either untreated (control) or treated with 200 mM NaCl for 6 h (left). SOD levels in wild-type (Col-0) and *ppr40-1* mutant cell suspensions (cells) and mitochondria (mit) isolated from wild-type (Col-0) and *ppr40-1* cells (right).

stress responses, and adaptation to extreme environmental conditions (Mackenzie and McIntosh, 1999; Møller, 2001). However, so far no mutation has been characterized that affects the function of Complex III. This article demonstrates that *PPR40* is important for Complex III activity.

In our experiments Suc gradient fractionation followed by BN and SDS electrophoresis in combination with proteomic analysis showed that *PPR40* is associated with Complex III of the mitochondrial electron transport chain. Separation of Complex III by two independent methods, namely by Suc density gradient centrifugation and BN gel electrophoresis, did not disrupt stable association of *PPR40*-HA with Complex III. However, electroelution of Complex III followed by

immunoprecipitation with a monoclonal anti-HA antibody did not pull down *PPR40*-HA (data not show), indicating that the C-terminal HA tag of *PPR40*-HA protein is hidden in Complex III. We have also tried complementing the *ppr40-1* mutant with a HA-*PPR40* construct, which carries an N-terminal HA-tag. However, this protein proved to be unstable and was never detected in the mitochondrial fraction, probably because the N-terminal HA tag interferes with mitochondrial import of *PPR40*. In conclusion, our data demonstrate that *PPR40*-HA is firmly associated with Complex III in nonstoichiometric amount. This observation is supported by the data showing that the *ppr40* mutations lead to reduction but not to complete loss of Complex III activity. This suggests that *PPR40* is an important regulator of cytochrome *c* reductase activity of Complex III, which is essential for mitochondrial electron transport and oxidative phosphorylation, but does not represent a core Complex III subunit. How *PPR40* regulates Complex III by molecular interactions with its core subunits remains to be resolved by further crystallization and structural studies.

Although several PPR proteins were reported to control organellar RNA processing, we could not find significant alterations in splicing and abundance of mitochondrial and nuclear transcripts encoding subunits of electron transport complexes I, III, and IV. However, comparative analysis of mitochondrial electron transport complexes clearly showed that subunit stoichiometry and abundance of Complex III in mutant and wild-type mitochondria was not significantly different suggesting that the *ppr40* mutation influences the activity and not the composition of Complex III.

The *PPR40* protein carries two separate domains of five and nine tandem PPR repeats. We have isolated two *ppr40* mutant alleles that differently affect leaf rosette development and ABA sensitivity of plants correlating with the position of T-DNA insertions in the *PPR40* gene. The T-DNA insertion in the *ppr40-1* allele is located upstream of the PPR-repeat coding domains and allows the synthesis of a 3'-truncated transcript, which is predicted to encode a protein lacking PPR repeats. In the *ppr40-2* mutant that displays less severe alterations of developmental and stress responses, the T-DNA insertion permits the synthesis of a longer truncated transcript that encodes a C-terminally truncated protein retaining the first domain of five PPR repeats. Leaky phenotype of the *ppr40-2* mutant suggests that the predicted *PPR40-2* protein is likely produced and partially functional, whereas *ppr40-1* represents a genuine null mutation causing a complete loss of *PPR40* function.

Reduction of respiration rate in the *ppr40-1* mutant suggests that the *PPR40* protein is important for proper function of Complex III, which has a cytochrome *c* reductase activity and catalyzes electron transfer from ubiquinone to cytochrome *c* in oxidative phosphorylation (Fig. 10). Complex III is a 500-kD multiprotein complex, which is partially embedded in the inner mitochondrial membrane (Berry et al., 2000)

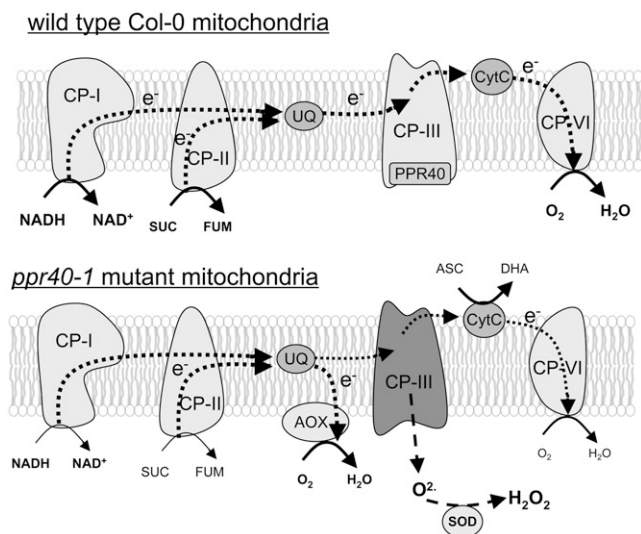


Figure 10. Proposed model for alteration of mitochondrial electron transport in the *ppr40-1* mutant compared to wild type. In wild-type mitochondria, electrons flow through either Complexes I-III-IV or Complexes II-III-IV consuming oxygen and producing water. NADH is an electron donor for Complex I, whereas succinate provides electrons for Complex II. In the *ppr40-1* mutant, the electron flow is reduced by dysfunction of Complex III enhancing the use alternative substrates of Complex IV, such as ascorbate. Reduced Complex III generates excess electrons producing superoxide, which is converted to hydrogen peroxide by MnSOD. AOX can contribute to the electron flow reducing the electron excess and superoxide pool.

and can form dynamic supercomplexes with Complexes I and IV (Krause et al., 2004; Dudkina et al., 2006). Antimycin A blocks the electron flow through inhibition of Complex III leading to overreduction of the ubiquinone pool and upstream respiratory Complexes I and II. As a consequence, electrons are transferred to molecular oxygen forming reactive superoxide anions (Møller, 2001; Navrot et al., 2007). Plant respiration employs alternative enzymes and electron substrates, which can bypass such disturbance of the main respiratory pathway (Mackenzie and McIntosh, 1999; Krause et al., 2004). We have found that impaired electron transport through Complex III in the *ppr40-1* mutant is accompanied by enhanced cytochrome *c* reductase activity of Complex IV, which probably uses alternative electron donors, such as ascorbate (Szarka et al., 2007). Enhanced ascorbate consumption of *ppr40-1* mutant shows that such alternative electron donors are in fact used in vivo to sustain oxidative respiration (Fig. 10).

Changes of ROS Regulation in the *ppr40-1* Mutant

Complex III is a principal source of ROS and inhibition of cytochrome *c* reductase activity increases ROS generation and oxidative damage (Chen et al., 2003). The defective cytochrome *c* pathway in the *ppr40-1* mutant is therefore predicted to enhance the production of superoxide ions, which can subsequently be converted

to H_2O_2 by MnSOD. We found that MnSOD activity compared to wild type is 40% higher in *ppr40-1* mitochondria, indicating enhanced H_2O_2 production. This logically correlates with an elevated level of lipid peroxidation in the *ppr40-1* mutant.

In plants, mitochondrial ROS production is effectively reduced by nonphosphorylating respiratory pathways, which include AOXs. AOX diverts the electron flow from the ubiquinone pool to oxygen and produces water without ATP production (Vanlerberghe and Ordog, 2002; Millenaar and Lambers, 2003). AOX activity thus bypasses the functions of Complexes III and IV of electron transport chain, and therefore, alleviates ROS formation during oxidative stresses (Maxwell et al., 1999). Inhibition of Complex III by antimycin A is reported to result in rapid activation of AOX1 genes (Vanlerberghe and McIntosh, 1994). In Arabidopsis, this typical stress response is controlled by transcriptional up-regulation of key AOX genes *AOX1a* and *AOX1d* (Clifton et al., 2006). We found that *AOX1d* transcript levels are 15- to 20-fold higher in the *ppr40-1* mutant compared to wild type even in the absence of stress exposure, which suggests *ppr40-1*-dependent activation of nonphosphorylating respiratory pathways due to impeded Complex III function. Observation of increased levels of H_2O_2 , MnSOD activity and lipid peroxidation in the *ppr40-1* mutant indicates that AOX activation cannot fully compensate the deficiency of COX. In addition, we observed that the *ppr40-1* mutant shows significantly enhanced sensitivity to the ROS generating herbicide paraquat and to externally employed hydrogen peroxide. This finding strongly suggests that the detoxification system of *ppr40-1* is overwhelmed by ROS, which is generated by the damaged mitochondrial electron transport, and that detoxification is insufficient to reduce the increased ROS levels effectively during stress conditions. Therefore, enhanced sensitivity of the *ppr40-1* mutant to high salinity probably also reflects enhanced ROS damage during stress.

Mitochondria with reduced respiration may generate a permanent stress condition by producing ROS as a constitutive stress signal for activation of cellular defense responses. This appears to be the case in the *ppr40-1* mutant, which is more sensitive to salinity, osmotic, and oxidative stress. The *ppr40-1* mutation causes reduced electron transport through Complex III and we found that this leads to increased use of alternative electron donors (downstream Complex III), such as ascorbate, by Complex IV (Fig. 10).

It is notable that the *ppr40-1* mutant displays acceleration of ABA-stimulated stomatal closure correlating with its enhanced sensitivity to ABA. Nonetheless, our efforts to associate the PPR40 function with correlative changes in the expression of key transcription factors of ABA-regulated stress response pathways did not provide a clear result. This, together with the above-discussed evidences, supports our conclusion that hypersensitivity of the *ppr40-1* mutant to ABA and salt is caused by a mitochondrial defect resulting in

enhancement of ROS generation and possible limitation of ATP production. ROS signaling is not only prominently linked to the control of programmed cell death (Gechev et al., 2006), but demonstrated to affect the regulation of stomatal closure by calcium and ABA signaling (Price et al., 1994; Leung and Giraudat, 1998; Finkelstein and Rock, 2002). ROS is also implicated in the control of calcium signals in ionic stress responses (Liu and Zhu, 1998; Laloi et al., 2004) and activation of a mitogen-activated protein kinase cascade involved in cross talk between biotic and abiotic stress signaling pathways (Kovtun et al., 2000). Combination of *ppr40-1* with known mutations implicated in ROS-related control of these pathways thus offers a suitable tool for answering the question how functions involved in mitochondrial electron transport control the generation of ROS and thereby influence different stress signaling pathways.

MATERIALS AND METHODS

Plant Materials and Growth Conditions

Arabidopsis (*Arabidopsis thaliana*) growth conditions in sterile culture and controlled growth chambers were as described earlier (Koncz et al., 1994). NaCl, sugar, ABA, and other compounds were added to the germination medium at concentrations indicated in the text. In all experiments, at least 100 seeds or seedlings were used per treatment. Plant growth was tested on vertical 1.5% agar plates. Root growth was monitored at daily intervals. Each experiment was repeated three times. Plant transformation was performed using the in planta *Agrobacterium* infiltration method (Bechtold et al., 1993). Stress treatments were carried out with 3-week-old in vitro cultured plants by placing them into liquid medium supplemented with either 150 or 200 mM NaCl. *Arabidopsis* cell suspensions were established, maintained, and transformed as described (Ferrando et al., 2000).

Identification and Characterization of Insertion Mutations

The T-DNA tagged *ppr40-1* and *ppr40-2* insertion mutants were identified in the Szeged (<http://www.szbk.u-szeged.hu/~arabidop>; Szabados et al., 2002) and Salk Institute (<http://signal.salk.edu/cgi-bin/tdnaexpress>) collections, respectively. Segregation analysis was performed using T2 and T3 families. To follow segregation of insertion mutant alleles, T-DNA specific primers homologous to the left border (Lba1) and gene-specific PCR primers (PPR-F and PPR-R2) were used in combinations. The presence of wild-type allele was confirmed by PCR amplification using gene-specific primers (see Supplemental Table S1).

RNA Isolation and Analysis

Total RNA was isolated from 3-week-old seedlings using the Tri-reagent extraction method (Chomczynski and Sacchi, 1987). Transcript levels were monitored by real-time (qRT-PCR) and semiquantitative RT-PCR analyses. cDNA templates were generated from DNase-treated (Promega) total RNA (2 μ g) samples by RT using SuperScript II RNase H⁻ reverse transcriptase (Invitrogen). Real-time RT-PCR reactions were prepared with SYBR Green JumpStart Taq ReadyMix (Sigma) employing the following protocol: denaturation 95°C/10 min, 40 to 45 cycles of 95°C/10 s and 60°C/1 min, with ABI PRISM 7700 sequence detection system (Applied Biosystems). Semiquantitative PCR reactions were performed in 50- μ L volume, using 0.2 μ g of cDNA template and Dupla-Taq polymerase (Zenon Bio, Szeged) employing the following protocol: denaturation 94°C/2 min, 35 cycles of 94°C/30 s, 60°C/45 s, and 72°C/1 min. Northern hybridization with a 1-kb radiolabeled cob probe amplified by the cob-F2 and cob-R primers was performed as described

by Brandt et al. (1993). The gene-specific primers are listed in Supplemental Table S2.

Computer Analysis

Searches for putative protein targeting signals were performed using the TargetP (<http://www.cbs.dtu.dk/services/TargetP>), Predotar (<http://urgi.infobiogen.fr/predotar/>), and iPSORT (<http://psort.nibb.ac.jp/>) algorithms. PCR primers were designed with the Primer3 software (http://biotools.umassmed.edu/bioapps/primer3_www.cgi). Multiple sequence alignments were generated using the ClustalW program (<http://www.ebi.ac.uk/clustalw/index.html>, <http://align.genome.jp>). Protein domain analyses were performed with the SMART service (<http://smart.embl-heidelberg.de/>).

Preparation of Mitochondria and Protein Isolation and Detection

Intact mitochondria were isolated from either 1-week-old cell suspension cultures or 3-week-old in vitro grown seedlings, or 4-week-old liquid root cultures using the method described by Werhahn et al. (2001). From 100 g of cell suspension, 100 mg of intact mitochondria was obtained and stored at -80°C. Protein purification (10–50 μ g) for immunoblot analysis was performed from frozen samples using 0.5% SDS in RIPA buffer (150 mM NaCl, 50 mM Tris-HCl, pH 7.5). The protein samples were separated by SDS-PAGE, blotted to polyvinylidene fluoride filters (Millipore), then incubated with a peroxidase-coupled monoclonal anti-HA antibody (Roche). The HA epitope-tagged proteins were detected using the Lumi-Light western blotting substrate (Roche).

Sucrose Gradient Centrifugation

Separation of mitochondrial protein complexes by Suc gradient ultracentrifugation was performed according to Dudkina et al. (2005). Freshly prepared mitochondria (40 mg) from PPR40-HA-expressing cell suspension culture were solubilized in a buffer containing 30 mM HEPES (pH 7.4), 150 mM potassium acetate, 10% glycerol, and 5% digitonin. The isolated protein extract was transferred onto an 11-mL linear Suc gradient (0.3–1.5 M Suc) and centrifuged at 150,000g for 20 h. Fractions (800 μ L) were collected from the gradient and 100 μ L aliquot of each fraction was analyzed by BN-PAGE and western blotting as described below.

BN-PAGE and SDS-PAGE

The analysis of mitochondrial complexes was performed as described (Wittig et al., 2006). Solubilization of mitochondria was carried out in a solution containing 50 mM NaCl, 50 mM imidazole-HCl (pH 7.3), 2 mM 6-aminohexanoic acid, 1 mM EDTA, and 6 g of digitonin (Fluka) to 1 g of protein. Protein (0.5 to 1 mg) was loaded in each lane of separating gels. In the case of BN-PAGE, the protein samples were separated in 4% to 13% acrylamide gradient gel, then GelCode Blue Stain Reagent was used for visualization of protein complexes. In the case of second-dimensional SDS-PAGE, the protein samples were separated in 8% to 16% acrylamide gradient gel, and then either the whole gel or a cut gel strip was used. The separated protein bands were visualized by SYPRO Ruby protein gel stain (Sigma). Quantitative analysis of photographed images was performed by densitometric evaluation using the ImageJ software (<http://rsb.info.nih.gov/ij/>).

Protein Identification by MS

In-gel digestion was performed as described in <http://donatello.ucsf.edu/ingel.html>. For liquid chromatography-tandem MS (LC-MS/MS) analysis, samples were analyzed on an Agilent 1100 nanoLC system on-line coupled to an XCT Plus ion trap mass spectrometer in information-dependent acquisition mode: MS acquisitions were followed by three collision-induced dissociation analyses on computer-selected multiply charged ions. For the database search, raw data were converted into a Mascot generic file with the DataAnalysis for LC/MSD Trap v3.2 software. The resulting MS and MS/MS data were searched using the Mascot v2.1 software (www.matrixscience.com) against the SwissProt 51.7 nonredundant database without species restriction (259,034 sequences) and the Protein Prospector Batchtag (v5.0.0.beta1) search engine

against the Uniprot (2006.10.21) database with Arabidopsis species restriction (49,487 entries); subsequently the data were also manually inspected.

Immunocytochemistry

Cultured cells transformed with the PPR40-HA construct were digested for 4 h with an enzyme mixture containing 1% (w/v) cellulase Onozuka R-10 (Yakult), 0.5% (w/v) Macerozyme R-10 (Yakult), and 0.16% (w/v) Driselase (Sigma) in B5 media supplemented with 0.4 M mannitol. Before the fixation procedure, cells were treated with 100 nM MitoTracker Orange (Molecular Probes). Cells were fixed with 3.7% (w/v) formalin in microtubule stabilizing buffer (50 mM PIPES [pH 6.9], 5 mM MgSO₄, 5 mM EGTA) for 1 h at room temperature (Ferrando et al., 2000). Following washing with 0.01 M phosphate-buffered saline (pH 7.2), cells were attached to poly-L-Lys (Sigma) coated slides and were extracted for 20 min with 0.5% (v/v) Triton-X-100. Mouse monoclonal anti-HA antibody (Sigma) was applied as 1:200 dilution in phosphate-buffered saline for 2 h at 37°C. After washing out the primary antibody, Alexa-488-conjugated secondary antibody (Molecular Probes) was added for 1 h at 37°C at 1:800 dilution and cells were mounted with Citofluor (Ted Pella). Cytological analyses were carried out using an Olympus FV1000 confocal laser scanning microscope (Olympus) with an oil-immersion Plan NeoFluar 60× objective.

Plasmid Constructions

The full-length cDNA of *At3g16890* gene was isolated by PCR amplification with ppr40F and ppr40R3 primers (Supplemental Table S2) and the PCR product was cloned as a *NcoI*-*Bgl*III fragment in the pPILY HA-epitope fusion vector (Ferrando et al., 2000). The PPR40-HA expression cassette was moved as a *NofI*-*SacI* fragment into the *SmaI*-*SacI* sites of pBIN19 (Bevan, 1984). The resulting binary vector was used for *Agrobacterium*-mediated transformation.

Determination of Chlorophyll Content

Samples (0.05 to 0.1 g) of 3-week-old in vitro grown control and treated seedlings were homogenized in liquid nitrogen and extracted with 80% (v/v) acetone for 2 h. The homogenate was centrifuged at 15,000g for 10 min. Absorption of the extracts was measured at 663 and 645 nm and the concentration of extracted chlorophylls was calculated according to Lichtenthaler (1987).

Enzyme Assays

SOD activity was assayed by the inhibition of photochemical reduction of nitroblue tetrazolium as described (Dhindsa et al., 1981). One unit of SOD activity was defined as the amount of enzyme required to cause 50% inhibition of reduction of nitroblue tetrazolium measured at 560 nm. The COX assay was performed as described by Szarka et al. (2004). Statistical analyses (one-way and two-way ANOVA and Student's *t* tests) were performed using the SPSS software version 13.0.1 (SPSS). H₂O₂ was detected by an endogenous peroxidase-dependent in situ histochemical staining procedure with DAB (Ren et al., 2002). The quantitative analysis was performed by scanning the images of stained leaves using densitometric evaluation (ImageJ software; <http://rsb.info.nih.gov/ij/>). Lipid peroxidation was measured in leaves using the thiobarbituric acid test, which determines malondialdehyde (MDA) as an end-product of lipid peroxidation (Sunkar et al., 2003). The amount of MDA was calculated using the difference of A₅₃₅ and A₇₃₀, and its extinction coefficient 155 mm⁻¹ cm⁻¹. Average values and SD were calculated from three or more independent experiments. Differences between means were determined by Duncan's multiple range test and labeled in all diagrams by different letters.

Stomata Opening Assay

Stomata opening assays were performed with epidermal peels from rosette leaves of 4- to 6-week-old plants (Leymarie et al., 1998). Before the measurements, plants were kept in dark for 3 h. The peels were floated in a solution containing 25 mM KCl and 10 mM MES-Tris (pH 6.15) for 1 h in the light and subsequently treated with different concentrations of ABA for 3 h. Stomatal pores were measured with a Nikon ECLIPSE TE300 microscope.

Measurement of Ascorbate Consumption and Respiration in Mitochondria

Ascorbate consumption was measured by reverse-phase HPLC as described (Szarka et al., 2002). The isocratic analyses were carried out with a Perkin Elmer Series 200 separation module and Perkin Elmer Series 200 diode array detector at 254 nm. The separations were performed using a Teknokroma Nucleosil 100 C18 column (average particle size, 5 μm, 25 cm × 4.6 mm). Respiratory measurements were carried out according to Ho et al. (2007) with slight modifications. To measure respiration of isolated mitochondria, 250 μg of mitochondrial protein was added to 1 mL of reaction mixture (0.3 M mannitol, 10 mM MOPS, 5 mM KH₂PO₄, 10 mM NaCl, 2 mM MgSO₄, 1% bovine serum albumin, pH 7.5). Oxygen consumption was measured at 25°C by a Clarke-type oxygen electrode (Hansatech Oxytherm). Reagents and inhibitors were added to the reaction in the following final concentrations: NADH (1.5 mM), succinate (5 mM), pyruvate (5 mM), ADP (0.3 mM), ATP (0.3 mM), rotenone (10 μM), antimycin A (10 mM), KCN (1 mM), salicylhydroxamic acid (2 mM), ascorbate (1 mM), and dithiothreitol (2 mM). Succinate or NADH-dependent respiration was measured both in the presence and absence of ADP. AOX was measured in the presence of succinate, NADH, ATP, ADP, pyruvate, and dithiothreitol to maximize electron flux and KCN was added to block cytochrome *c* pathway. Salicylhydroxamic acid was added to ensure that the oxygen consumption measured was due to AOX activity. Ascorbate-dependent respiration was measured after the addition of antimycin A to block the electron flow through Complex III.

Measurement of H₂O₂ Production

Hydrogen peroxide generation was measured according to Dlasková et al. (2006), using the Amplex Red Hydrogen Peroxide/Peroxidase Assay Kit (A22188; Invitrogen, Molecular Probes). Isolated mitochondria (0.3 mg) were suspended in 10 mM K-phosphate buffer (pH 7.2) supplemented with 0.4 M mannitol, respiratory substrates (5 mM Glu, 5 mM succinate, 5 mM malate, and 1 mM ascorbate), 0.2 units mL⁻¹ horseradish peroxidase, and 50 μM Amplex Red reagent and incubated at room temperature (25°C) for 30 min. The accumulation of resorufin was determined spectrophotometrically at 560 nm (Multiskan Spectrum; Thermo Labsystems).

Determination of ABA Content

For determination of ABA content, we used an ELISA (Phytoetek-ABA; Sigma-Aldrich) assay. (100 mg). Grinded plant samples (100 mg) were extracted with 5 mL of cold mixture of 100 mM NaHCO₃:methanol (80:20, v/v) containing 1 mg of butylated hydroxytoluene in a volume of 100 mL. The extraction procedure was performed twice at 4°C for 24 h each, and then the solvent was evaporated. This assay utilizes monoclonal antibody for ABA, and the determination of (+)-cis-ABA in the plant extract is based on the competitive binding of ABA and the tracer (alkaline phosphatase-labeled ABA) to the antibody-coated microwells.

Supplemental Data

The following materials are available in the online version of this article.

Supplemental Figure S1. Sequence comparisons of the PPR40 protein.

Supplemental Figure S2. PPR40 transcript levels in wild type, *ppr40-1* mutant, and genetically complemented *ppr40-1* lines.

Supplemental Figure S3. Transcript levels of stress- and ABA-induced genes in wild-type plants and in the *ppr40-1* mutant.

Supplemental Figure S4. Densitometric analysis of respiratory complexes and components of Complex III in wild-type and *ppr40-1* mutant mitochondria.

Supplemental Figure S5. Multiple alignment showing editing in *cob* sequences obtained from reverse transcript amplification of the *ppr40-1* mutant and wild-type plants.

Supplemental Table S1. Germination and growth conditions used for characterization of the *ppr40-1* mutant phenotype.

Supplemental Table S2. Oligonucleotides used in this study.

ACKNOWLEDGMENTS

We thank Annamária Király and Mónika Kispéterné Gál for their technical assistance, Mihály Dobó for growing the plants, Dr. Péter Doró and Miklós Mocsonoky for their help in bioinformatic analyses, and Dr. Irma Tari for her help in the ABA measurements.

Received October 20, 2007; accepted February 20, 2008; published February 27, 2008.

LITERATURE CITED

- Andrés C, Lurin C, Small ID (2007) The multifarious roles of PPR proteins in plant mitochondrial gene expression. *Physiol Plant* **129**: 14–22
- Bechtold N, Ellis J, Pelletier G (1993) In planta *Agrobacterium* mediated gene transfer by infiltration of adult *Arabidopsis thaliana* plants. *C R Acad Sci III* **316**: 1194–1199
- Berry EA, Guergova-Kuras M, Huang LS, Crofts AR (2000) Structure and function of cytochrome bc complexes. *Annu Rev Biochem* **69**: 1005–1075
- Bevan M (1984) Binary *Agrobacterium* vectors for plant transformation. *Nucleic Acids Res* **12**: 8711–8721
- Blatch GL, Lässle M (1999) The tetratricopeptide repeat: a structural motif mediating protein-protein interactions. *Bioessays* **21**: 932–939
- Brandt P, Unseld M, Eckert-Ossenkopp U, Brennicke A (1993) An rps14 pseudogene is transcribed and edited in *Arabidopsis* mitochondria. *Curr Genet* **24**: 330–336
- Chen Q, Vazquez EJ, Moghaddas S, Hoppel CL, Lesnefsky EJ (2003) Production of reactive oxygen species by mitochondria: central role of complex III. *J Biol Chem* **278**: 36027–36031
- Chomczynski P, Sacchi N (1987) Single-step method of RNA isolation by acid guanidinium thiocyanate-phenol-chloroform extraction. *Anal Biochem* **162**: 156–159
- Clifton R, Millar AH, Whelan J (2006) Alternative oxidases in *Arabidopsis*: a comparative analysis of differential expression in the gene family provides new insights into function of non-phosphorylating bypasses. *Biochim Biophys Acta* **1757**: 730–41
- Desikan R, A-H-Mackerness S, Hancock JT, Neill SJ (2001) Regulation of the *Arabidopsis* transcriptome by oxidative stress. *Plant Physiol* **127**: 159–172
- Desloire S, Gherbi H, Laloui W, Marhadour S, Clouet V, Cattolico L, Falentin C, Giancola S, Renard M, Budar F, et al (2003) Identification of the fertility restoration locus, Rfo, in radish, as a member of the pentatricopeptide-repeat protein family. *EMBO Rep* **4**: 588–594
- Dhindsa RA, Plumb-Dhindsa P, Thorpe TA (1981) Leaf senescence: correlated with increased permeability and lipid peroxidation, and decreased levels of superoxide dismutase and catalase. *J Exp Bot* **126**: 93–101
- Dlasková A, Špaček T, Škobisová E, Šantorová J, Ježek P (2006) Certain aspects of uncoupling due to mitochondrial uncoupling proteins in vitro and in vivo. *Biochim Biophys Acta* **1757**: 467–473
- Dudkina NV, Eubel H, Keegstra W, Boekema EJ, Braun HP (2005) Structure of a mitochondrial supercomplex formed by respiratory-chain complexes I and III. *Proc Natl Acad Sci USA* **102**: 3225–3229
- Dudkina NV, Heinemeyer J, Sunderhaus S, Boekema EJ, Braun HP (2006) Respiratory chain supercomplexes in the plant mitochondrial membrane. *Trends Plant Sci* **11**: 232–240
- Ferrando A, Farràs R, Jasik J, Schell J, Koncz C (2000) Intron-tagged epitope: a tool for facile detection and purification of proteins expressed in *Agrobacterium*-transformed plant cells. *Plant J* **22**: 1–8
- Finkelstein RR, Rock CD (2002) Abscisic acid biosynthesis and response. In CR Somerville, EM Meyerowitz, eds, *The Arabidopsis Book*. American Society of Plant Biologists, Rockville, MD, doi: 10.1199/tab.0058, www.aspb.org/publications/arabidopsis/
- Gechev TS, Van Breusegem F, Stone JM, Denev I, Laloi C (2006) Reactive oxygen species as signals that modulate plant stress responses and programmed cell death. *Bioessays* **28**: 1091–101
- Giegé P, Brennicke A (1999) RNA editing in *Arabidopsis* mitochondria effects 441 C to U changes ORFs. *Proc Natl Acad Sci USA* **96**: 15324–15329
- Gutierrez S, Sabar M, Lelandais C, Chetrit P, Diolez P, Degand H, Boutry M, Vedel F, de Kouchkovsky Y, De Paep R (1997) Lack of mitochondrial and nuclear-encoded subunits of complex I and alteration of the respiratory chain in *Nicotiana glauca* mitochondrial deletion mutants. *Proc Natl Acad Sci USA* **94**: 3436–3441
- Gutierrez-Marcos JF, Dal Pra M, Giulini A, Costa LM, Gavazzi G, Cordelier S, Sellam O, Tatout C, Paul W, Perez P, et al (2007) Empty pericarp4 encodes a mitochondrial-targeted pentatricopeptide repeat protein necessary for seed development and plant growth in maize. *Plant Cell* **19**: 196–210
- Heazlewood JL, Tonti-Filippini JS, Gout A, Day DA, Whelan J, Millar AH (2004) Experimental analysis of the *Arabidopsis* mitochondrial proteome highlights signaling and regulatory components, provides assessment of targeting prediction programs, and points to plant specific mitochondrial proteins. *Plant Cell* **16**: 241–256
- Ho LHM, Giraud E, Lister R, Thirkettle-Watts D, Low J, Clifton R, Howell KA, Carrie C, Donald T, Whelan J (2007) Characterization of the regulatory and expression context of an alternative oxidase gene provides insights into cyanide-insensitive respiration during growth and development. *Plant Physiol* **143**: 1519–1533
- Koncz C, Martini N, Szabados L, Hrouda M, Bachmair A, Schell J (1994) Specialized vectors for gene tagging and expression studies. In S Gelvin, B Schilperoort, eds, *Plant Molecular Biology Manual*, B2. Kluwer Academic, Dordrecht, The Netherlands, pp 1–22
- Kovtun Y, Chiu WL, Tena G, Sheen J (2000) Functional analysis of oxidative stress-activated mitogen-activated protein kinase cascade in plants. *Proc Natl Acad Sci USA* **97**: 2940–2945
- Krause E, Reifschneider NH, Vocke D, Seelert H, Rexroth S, Dencher NA (2004) “Respirasome”-like supercomplexes in green leaf mitochondria of spinach. *J Biol Chem* **279**: 48369–48375
- Laloi C, Apel K, Danon A (2004) Reactive oxygen signalling: the latest news. *Curr Opin Plant Biol* **7**: 323–328
- Lee BH, Lee H, Xiong L, Zhu JK (2002) A mitochondrial complex I defect impairs cold-regulated nuclear gene expression. *Plant Cell* **14**: 1235–51
- Leung J, Giraudat J (1998) Abscisic acid signal transduction. *Annu Rev Plant Physiol Plant Mol Biol* **49**: 199–222
- Leymarie J, Vasseur A, Lascève G (1998) CO₂ sensing in stomata of *abi1-1* and *abi2-1* mutants of *Arabidopsis thaliana*. *Plant Physiol Biochem* **36**: 539–543
- Lichtenthaler HK (1987) Chlorophylls and carotenoids: pigments of photosynthetic biomembranes. *Methods Enzymol* **148**: 350–382
- Liu J, Zhu JK (1998) A calcium sensor homolog required for plant salt tolerance. *Science* **280**: 1943–1945
- Liu S, Zhang C, Zhou Y (2005) Domain graph of *Arabidopsis* proteome by comparative analysis. *J Proteome Res* **4**: 435–444
- Lurin C, Andres C, Aubourg S, Bellaoui M, Bitton F, Bruyere C, Caboche M, Debast C, Gualberto J, Hoffmann B, et al (2004) Genome-wide analysis of *Arabidopsis* pentatricopeptide repeat proteins reveals their essential role in organelle biogenesis. *Plant Cell* **16**: 2089–2103
- Mackenzie S, McIntosh L (1999) Higher plant mitochondria. *Plant Cell* **11**: 571–586
- Maxwell DP, Wang Y, McIntosh L (1999) The alternative oxidase lowers mitochondrial reactive oxygen production in plant cells. *Proc Natl Acad Sci USA* **96**: 8271–8276
- Meierhoff K, Felder S, Nakamura T, Bechtold N, Schuster G (2003) HCF152, an *Arabidopsis* RNA binding pentatricopeptide repeat protein involved in the processing of chloroplast psbB-psbT-psbH-petB-petD RNAs. *Plant Cell* **15**: 1480–1495
- Millenaar FF, Lambers H (2003) The alternative oxidase: in vivo regulation and function. *Plant Biol* **5**: 2–15
- Møller IM (2001) Plant mitochondria and oxidative stress: electron transport, NADPH turnover, and metabolism of reactive oxygen species. *Annu Rev Plant Physiol Plant Mol Biol* **52**: 561–591
- Navrot N, Rouhieh N, Gelhaye E, Jacquot JP (2007) Reactive oxygen species generation and antioxidant systems in plant mitochondria. *Physiol Plant* **129**: 185–195
- Newton KJ, Coe EH (1986) Mitochondrial DNA changes in abnormal growth (nonchromosomal stripe) mutants of maize. *Proc Natl Acad Sci USA* **83**: 7363–7366
- Oguchi T, Sage-Ono K, Kamada H, Ono M (2004) Genomic structure of a novel *Arabidopsis* clock-controlled gene, AtC401, which encodes a pentatricopeptide repeat protein. *Gene* **330**: 29–37
- Perales M, Eubel H, Heinemeyer J, Colaneri A, Zabaleta E, Braun HP (2005) Disruption of a nuclear gene encoding a mitochondrial gamma carbonic anhydrase reduces complex I and supercomplex I+III₂ levels and alters mitochondrial physiology in *Arabidopsis*. *J Mol Biol* **350**: 263–277
- Plaxton WC, Podestá FE (2006) The functional organisation and control of plant respiration. *Crit Rev Plant Sci* **25**: 159–198

- Price AH, Taylor A, Ripley SJ, Griffiths A, Trewavas AJ, Knight MR (1994) Oxidative signals in tobacco increase cytosolic calcium. *Plant Cell* **6**: 1301–1310
- Raghavendra AS, Padmasree K (2003) Beneficial interactions of mitochondrial metabolism with photosynthetic carbon assimilation. *Trends Plant Sci* **8**: 1360–1385
- Ren D, Yang H, Zhang S (2002) Cell death mediated by MAPK is associated with hydrogen peroxide production in *Arabidopsis*. *J Biol Chem* **277**: 559–565
- Siedow JA, Day DA (2000) Respiration and photorespiration. In BB Buchanan, W Gruissem, RL Jones, eds, *Biochemistry and Molecular Biology of Plants*. American Society of Plant Physiologists, Rockville, MD, pp 676–728
- Small ID, Peeters N (2000) The PPR motif—a TPR-related motif prevalent in plant organellar proteins. *Trends Biochem Sci* **25**: 46–47
- Sunkar R, Bartels D, Kirch HH (2003) Overexpression of a stress-inducible aldehyde dehydrogenase gene from *Arabidopsis thaliana* in transgenic plants improves stress tolerance. *Plant J* **35**: 452–464
- Sweetlove LJ, Fait A, Nunes-Nesi A, Williams T, Fennie AR (2007) The mitochondrion: an integration point of cellular metabolism and signaling. *Crit Rev Plant Sci* **26**: 17–43
- Szabados L, Kovács I, Oberschall A, Abrahám E, Kerekes I, Zsigmond L, Nagy R, Alvarado M, Krasovskaja I, Gál M, et al (2002) Distribution of 1000 sequenced T-DNA tags in the *Arabidopsis* genome. *Plant J* **32**: 233–242
- Szarka A, Horemans N, Bánhegyi G, Asard H (2004) Facilitated glucose and dehydroascorbate transport in plant mitochondria. *Arch Biochem Biophys* **428**: 73–80
- Szarka A, Horemans N, Kovács Z, Gróf P, Mayer M, Bánhegyi G (2007) Dehydroascorbate reduction in plant mitochondria is coupled to the respiratory electron transfer chain. *Physiol Plant* **129**: 225–232
- Szarka A, Stadler K, Jenei V, Margittai É, Csala M, Jakus J, Mandl J, Bánhegyi G (2002) Ascorbyl free radical and dehydroascorbate formation in rat liver endoplasmic reticulum. *J Bioenerg Biomembr* **34**: 317–323
- Vanlerberghe GC, McIntosh L (1994) Mitochondrial electron transport regulation of nuclear gene expression. Studies with the alternative oxidase gene of tobacco. *Plant Physiol* **105**: 867–874
- Vanlerberghe GC, Ordog SH (2002) Alternative oxidase: integrating carbon metabolism and electron transport in plant respiration. In GH Foyer, G Noctor, eds, *Advances in Photosynthesis and Respiration, Photosynthetic Nitrogen Assimilation and Associated Carbon and Respiratory Metabolism*, Vol 12. Kluwer Academic Publishers, Dordrecht, The Netherlands, pp 173–191
- Werhahn W, Niemeyer A, Jansch L, Kruff V, Schmitz UK, Braun HP (2001) Purification and characterization of the preprotein translocase of the outer mitochondrial membrane from *Arabidopsis*. Identification of multiple forms of TOM201. *Plant Physiol* **125**: 943–954
- Williams PM, Barkan A (2003) A chloroplast-localized PPR protein required for plastid ribosome accumulation. *Plant J* **36**: 675–686
- Wittig I, Braun HP, Schagger H (2006) Blue-native PAGE. *Nat Protocols* **1**: 416–428
- Yamaguchi-Shinozaki K, Shinozaki K (2005) Organization of cis-acting regulatory elements in osmotic- and cold-stress-responsive promoters. *Trends Plant Sci* **10**: 88–94